National Research Council Canada
Conseil national de recherches Canada

NATIONAL AERONAUTICAL ESTABLISHMENT

LABORATORY TECHNICAL REPORT

LTR - LA - 94

A SPIRE ARRAY FOR GENERATING THICK TURBULENT SHEAR LAYERS FOR NATURAL WIND SIMULATION IN WIND TUNNELS

N.M. STANDEN

RAPPORT TECHNIQUE DE LABORATOIRE

ÉTABLISSEMENT AÉRONAUTIQUE NATIONAL

MAY 1972

OTTAWA, CANADA

NATIONAL AERONAUTICAL ESTABLISHMENT

ÉTABLISSEMENT AÉRONAUTIQUE NATIONAL

CANADA

PAGES 18
PAGES

FIG. 24
DIAG.

REPORT
RAPPORT

LOW SPEED AERODYNAMICS
SECTION

REPORT LTR-LA-94
RAPPORT

DATE May 1972
DATE

LAB. ORDER NAE-1637
COMM. LAB.

FILE 49-7-47
DOSSIER

FOR Internal
POUR

REFERENCE
RÉFÉRENCE

LTR-LA-94

A SPIRE ARRAY FOR GENERATING THICK TURBULENT SHEAR LAYERS FOR NATURAL WIND SIMULATION IN WIND TUNNELS

SUBMITTED BY R. J. Templin
PRÉSENTÉ PAR
SECTION HEAD
CHEF DE SECTION

AUTHOR N. M. Standen
AUTEUR

APPROVED F. R. Thurston
APPROUVÉ
DIRECTOR
DIRECTEUR

FORM NRC 538
FORMULAIRE NRC 538

COPY NO.
COPIE NR.

1.0 BACKGROUND

The generation of thick shear layers in wind tunnels of conventional working section length has been investigated at the National Aeronautical Establishment during the past four years. Various mechanical devices, located at the working section entrance, have been used in the attempt to produce a shear layer of arbitrary depth which models certain properties of the atmospheric wind below about 1500 ft. altitude.

Such a simulation would permit the use of conventional wind tunnels in the study of various phenomena of current interest, including steady and unsteady wind loads on large urban structures, atmospheric diffusion, ventilation of cities and the effects of large structures and terrain features on downwind sites. Creation of shear layers with thicknesses up to half the tunnel test section height appears to be possible at this time, allowing large-scale, detailed models of structures and terrain features to be tested. At present, there is no provision in the NAE technique for modelling thermal gradients in the lower atmosphere. The simulation, therefore, is of a neutrally-stable, or high-speed wind atmospheric boundary layer. However, for certain problems, such as the wind loads on buildings, the high-speed wind case presents the most important condition. These problems may be studied with the present technique.

The properties of the wind which appear to be most important in modelling the high-speed wind case are the mean velocity variation with height (mean velocity profile), the turbulence intensity, especially the intensity of the longitudinal turbulence component, the power spectral density of the longitudinal component, and the Reynolds shear stress variation with height. Initially, the shear stress distribution was not considered, mainly because most available wind data provided only mean profiles, turbulence intensities and spectral densities.

References (1) and (2) describe the modelling considerations, some of the full-scale data used as comparisons and the initial tunnel tests on various shear-producing devices. Briefly, we selected a power law of the form $U/U_o = (Z/\delta)^{\alpha}$ to represent the mean velocity profile; for an urban wind the exponent α was set at about 0.35 or 0.40 and the total layer thickness δ was chosen to be about 1500 ft. (full scale). In the above expression, U is the mean velocity at height Z, and U_o is the gradient velocity at height δ.

The distribution of longitudinal turbulence intensity (based on free stream or gradient wind velocity) was expected to be similar to the data from Sale and Brookhaven as represented in Reference (1) and (2). The magnitude of this turbulence

intensity, however, was expected to be larger than suggested by these same data, since the urban wind develops over a rougher terrain. The von Karman distribution of the longitudinal turbulence power spectral density, in the form developed in Reference (1), was selected as the spectral model for the wind tunnel shear layer.

As a result of the tests reported in Reference (2), an array of standard half-width spires (Fig. 1), located across the entrance to the tunnel working section with one-half spire height spacing between individual spires, was selected as the most appropriate shear layer generator. The dimensions of this spire are given in Table I. Further tests were then conducted in which shear layers generated by these spires were the subject of investigation. The spire size was varied from the original 6 inches to a maximum of 7 feet, and the free stream wind velocity from 50 fps to 100 fps. Various modifications to the spires were also investigated, comprising patterns of holes in the spire, removed sections of the spire, and vertical splitter plates attached to the rear side of the spire. These spires and modifications are shown in Figures (2), (3) and (4).

2.0 TEST RESULTS AND DISCUSSION

The measurements in the shear layers behind the 6-inch and 12-inch spires were conducted in a 3-foot square tunnel with a smooth floor. The 4-foot and 7-foot spires

were installed in the NAE 30 foot V/STOL tunnel in the course of measurements on model buildings and cities. In these latter tests, the floor surface was covered with uniform cubes in regular, alternately staggered rows. The cubes were 3 inches per side behind the 4-foot spires and 6 inches per side behind the 7-foot spires. They were spaced at 12" and 24" centres, respectively. The array of cubes is referred to as the "roughness" in the remainder of this paper.

2.1 Mean Velocity Profile

The measured mean velocity profiles were plotted on log-log graphs in the form U/U_o versus height Z above the tunnel floor. Straight line approximations to the data point distributions on these graphs provide power law profiles. The intercept of the straight line approximation with the line $U/U_o = 1.0$ provides the value of δ to be used and the slope of the straight line yields the exponent α.

In Figure (5), the velocity profiles generated by the unmodified 6-inch spires of Ref. (2) are shown. The profiles were measured at three and six spire heights downstream of the spire row. The velocity profile at 18" behind one of the spires (Fig. 5a) is noteworthy because this type of profile occurred in many of the later tests. There appear to be two distinct regions in this profile, each of which may be approximated by straight lines on the log-log plot. The power

law exponents determined from the slopes of these lines are denoted α_L for the lower fit and α_u for the upper section. This double-profile velocity distribution is typical of a shear layer immediately downstream of a roughness change (Ref. 3).

It is interesting to note that the velocity profile between spires is very similar in depth and shape to the lower profile of the velocity distribution on the spire centerline. This suggests that not only is vertical adjustment of the shear layer incomplete at 3 spire heights downstream but that lateral mixing has not yet smoothed out the wake effect of the upper portion of the spire.

The velocity profiles between two spires and in line with one of the spires at a distance of 6 spire heights downstream of the spire row are shown in Fig. 5b. The difference in profiles between spires and behind a spire, referred to as the shadow effect in Ref. 2, is nearly eliminated, and the velocity distribution is easily represented by a single power law profile. The thickness of the shear layer is less than the spire height.

The addition of floor roughness behind the 6-inch spires resulted in the velocity profiles shown in Fig. 5c. One was measured at a distance of 36 inches behind the centre spire, the other at 18 inches. There is an indication of a

two-profile distribution in the 18 inch position. The extent of the lower profile region and the numerical values of the profile exponents are nearly identical to the values obtained without roughness at this station. At 36 inches downstream, the profile is well represented by a single power law, but the exponent is considerably higher than was found in the case of the smooth floor. It would appear that the shear layer had essentially eliminated discreet traces of the spire wake, but that the surface roughness was too severe to provide an exponent in the range $\alpha = 0.35$. The roughness consisted of staggered rows of inverted 1/4 inch diameter rivets, about 1/2 inch high and at a 3/4 inch spacing.

The velocity profiles 3 spire heights downstream of a row of 12-inch spires (Fig. 2) are shown in log-log form in Fig. 6. Again, the shadow effect is apparent in comparing the velocity profiles in line with a spire and between spires. The velocity distribution in line with the spire also displays the two-power law profile found with the 6-inch spires. Further, the exponent of the lower profile is essentially the same for both 6-inch and 12-inch spires, and the lower profile occupies about the bottom half of the boundary layer in each case. The holes in the 12-inch spires appear to have had little effect on the development of the velocity profile. No information has been obtained at a distance of 6 spire heights

downstream of the 12-inch spires.

The 4-foot spires, shown in Fig. 3, were installed in the 30 foot V/STOL tunnel in two separate tests. In both cases, the boundary layer measurements were taken 6 spire heights downstream of the spire row, and on a line passing between two spires. In one test, the floor of the tunnel was covered with the rows of 3-inch cubes from the spires to the measurement position. In the other test, a 1/400 scale model of the westerly section of downtown Montreal replaced eight feet of block roughness upstream of the measuring station.

Figure 7 shows the velocity profile in the simplest configuration, spires and roughness only. The two-profile distribution is evident, but the region of the lower profile is a smaller fraction of the spire height than was the case for the 6- and 12-inch spires at 3 spire heights. Moreover, the upper profile has very nearly the desired power law exponent. The same configuration, but with the city model installed, produced the velocity profile of Fig. 8. The two-profile character is more pronounced and is closer to that obtained with the 6- and 12-inch spires at 3 spire heights. Figures 7 and 8 suggest that the uniform block roughness created too rough a surface and prevented the shear layer from achieving a single-profile character with the desired exponent in its representative power law at a distance of 6 spire

heights downstream. The inclusion of the city model apparently increased the effective roughness, causing greater distortion of the profile.

In order to reduce the overall drag level of the spires, a splitter plate was attached on the downwind centreline of each spire. The splitter plate was shaped as a half spire (Fig. 3b) and was attached in such a way as to allow an arbitrary gap between the spire and the splitter plate. This modification, with a separation gap of 1 inch, together with the uniform block roughness (no city model), resulted in the velocity distribution of Fig. 9. This shows a notable improvement over the profile achieved without the splitter plates, Fig. 7. The lower profile in Fig. 9 was finally removed when 9 rows of the block roughness were removed, resulting in the profile shown in Fig. 10.

The 7-foot spires, together with splitter plates, shown in Fig. 4, were installed in the 30 foot V/STOL tunnel in the course of other tests. Uniform cubes, 6 inches a side, were used as floor roughness, following the same pattern as in the previous tests with the 4-foot spires. These spires had no holes or cut-out regions, and the splitter plates were right triangles, with a base length of 4 feet and 7 feet in height.

With only the spires, splitter plates and uniform roughness installed, the velocity profile at 5.8 spire heights

downstream was measured, as shown in Fig. 11. A two-profile distribution is apparent, but the lower profile is much smaller in extent, relative to the total thickness of the shear layer, than is the case with the other reported two-profile distributions. The predominant, upper profile is well approximated by a power law with exponent $\alpha = 0.19$. With a city model installed, similar to the model involved in Fig. 8 but twice the scale, the velocity distribution at the same measuring station is shown in Fig. 12. Here the distribution is essentially given by a single power law profile with exponent $\alpha = 0.34$.

2.2 Turbulence Intensity

The modelling of the turbulence intensity in the various shear layers was not subject to as stringent requirements as was the mean velocity profile. This was so mainly because no full-scale data reporting the turbulence intensity distributions through the urban shear layer were known. The longitudinal turbulence data reported by Davenport (Ref. 4) from Sale, Australia and Brookhaven, U.S.A., were replotted in Ref. 2 after assuming velocity profiles typical of surburban and open terrain. These data are reproduced in Fig. 13, which show the turbulence intensity distributions in the shear layers discussed in this paper.

Examining the curves in Fig. 13, there does not appear to be any strong readjustment of the intensity distribution

due to the addition or deletion of gross physical properties in the tunnel. In Fig. 13a, distance downstream of the 6-inch spires tends to smooth out the intensity distribution in the lower 40% of the boundary layer when floor roughness was present. The introduction of the roughness itself appeared also to reduce the sharp peak intensity of this region. Fig. 13b suggests that the intensity peaks, both of u' (longitudinal turbulence) and v' (vertical turbulence), become larger and more pronounced in the lower 40% when a city model is introduced. The same figure also shows a minor tendency for the profiles of turbulence intensities to be nearly constant from about 0.5δ to 0.7δ when the splitter plates are installed. On the other hand, Fig. 13c displays distributions of u' turbulence more closely comparable to the roughness cases in Fig. 13a. It should be recalled, however, that the splitter plates used in the 7-foot spires of Fig. 13c were of considerably different design than those used with the 4-foot spires of 13b.

If the present turbulence distributions are compared with the Case I data of Ref. 3, it is seen that all spire-generated shear layers, with combinations of roughness and/or city model, are more typical of the measurements downstream of the roughness change in Ref. 3 than upstream. The 7-foot spires with the thin splitter plates, with or without the city model,

appear to conform best to the far downstream data of Ref. 3 and to the data for Brookhaven, as depicted in Ref. 2.

2.3 Longitudinal Power Spectral Density

In Reference 1 the von Karman distribution for the power spectral density of the longitudinal component of turbulence was selected as a standard of comparison. In that paper the value of the non-dimensional frequency (independent variable) at the peak of the spectrum was calculated to be

$$\frac{L}{h}(N_p) = 0.145 \qquad (N_p = n_p h/U_r) \qquad (1)$$

where L is the integral scale of the u' turbulence, h is a reference length, taken in Ref. 1 to be the shear layer thickness, n_p is the frequency at the spectrum peak and U_r is a reference velocity. In Ref. 6 a relationship between N_p and altitude Z is obtained by Berman; in that paper, Berman defines N_p using local values of height and velocity

$$N_p = \frac{n_p Z}{U} = .005Z^{.75} \qquad (Z \text{ in meters}) \qquad (2)$$

In the measurements reported in this paper, two non-dimensional frequencies have been employed. In the shear layers produced by the 6-inch and 12-inch spires, the reference length in N_p was constant and equal to the spire height. This length was very nearly equal to the boundary layer thickness

at the measuring station. The reference velocity was taken to be the local mean velocity at the height of the measurement. In plotting the spectral densities measured in the 4-foot and 7-foot spire shear layers, fixed reference lengths and reference velocities were used. These corresponded to 800 feet altitude and the mean velocity at that altitude since the only calculation of wind spectra made from the full-scale Montreal measurements (Ref. 7) was based on data obtained at that location.

The calculated spectral densities are shown in Fig. 14. The -2/3 slope line included in the Figures is in reference to the slope of the von Karman distribution at frequencies above the peak. The slope of -2/3 is theoretically an asymptotic value, but in fact, the slope of the von Karman curve is very close to -2/3 immediately beyond the peak. The spectral densities in Fig. 14 agree well with this slope and with the +1:0 slope of the von Karman curve at very low frequencies. In Fig. 14f and 14g the full-scale Montreal spectral density from Ref. 7 is included. Agreement with the 4-foot spire data is good in Fig. 14e and 14f, and the 7-foot spire data (Fig. 14g) are equally acceptable if the peak of these data is shifted to the left to coincide with the full-scale peak.

The value of the peak non-dimensional frequency N_p for each of the curves shown is of some interest. Using the von Karman relationship at the peak (Equation 1), the integral scale L can be calculated from the given value of N_p. For the full-scale data from Montreal, the calculated value of integral scale, taking a value of N_p = .35 from Fig. 14f, is 331 feet. Berman's equation can be used to check the value of N_p obtained in the spectral analysis. From Equation 2, N_p = .309 for the Montreal case; thus Berman's relationship suggests an integral scale L = 375 feet. The location of the 7-foot spire spectra to the right of the full-scale data in Fig. 14g is indicative of an inappropriate integral scale in this modelling of the shear layer. Using the geometric scaling of 1:200, the tunnel model provided an integral scale L = 264 feet.

The wind tunnel spectra can be used to construct a relationship between peak frequency and altitude following Berman's treatment of the full-scale shear layers. Such a relationship would indicate whether a degree of similarity exists between the tunnel shear layers and the full-scale wind. Figure 15 shows the non-dimensional peak frequency based on local height and velocity, plotted against height. The heights at which measurements were made in the tunnel shear

layers have been converted to an equivalent full-scale height. In the cases of the 6-inch and 12-inch spires, this was accomplished by assuming that the height of the shear layer at the measuring station was equivalent to 1200 feet full scale. The effective height of the shear layer, directly behind the 12-inch spire, was taken to be 8 inches, which is the extrapolated height of the lower profile region of that shear layer (see Fig. 6). The 4-foot spire shear layers were scaled at 1:400 with the city model installed, and the 7-foot spire layers were scaled at 1:200 with the city model in. In each of the larger shear layers generated without the city model installed, the scaling was such that the shear layer depth was set equivalent to 1200 feet.

Examining Fig. 15, it is seen that most of the tunnel data lie above but roughly parallel to the relationship suggested by Berman. This is due to the fact that the integral scales of the longitudinal turbulence in the tunnel shear layers are smaller (after geometric scaling) than the values implied by the spectra used by Berman. The data used by Berman were measured in wind which had developed over open, treed or low suburban terrain. While some of the tunnel shear layers may be representative of such a surface condition, notably those tests which did not include a city model, there is very little difference between tunnel cases, with

or without a city model, in Fig. 15. Consequently, the discrepancies between the tunnel measurements and Berman's relationship should probably be argued on the basis of incorrect profiles and shear layer thicknesses in the wind tunnel models. Berman's equation might be altered by the inclusion of urban wind measurements, but the full-scale datum from Montreal, plotted in Fig. 15, does not suggest such an alteration.

3.0 CONCLUSIONS

In general, the spires appear to provide a good approximation to the atmospheric wind below about 1500 feet altitude, when considering the neutrally-stable or high wind velocity atmosphere. Some details of the spire design and use still need further refinement. However, the following observations seem to apply.

1. The profile given in Table I may be used to construct two-dimensional, solid spires of any arbitrary size. Such spires are suitable as the basic component in a wind simulation technique in wind tunnels.

2. The addition of a distributed roughness on the wind tunnel floor downstream of the spires, and the use of a thin triangular splitter plate on the downstream side of the spire are necessary to achieve certain predetermined properties of the shear layer at a measuring station in a given model.

The amount of roughness and the location and size of the splitter plate relative to the spire may require adjustment to obtain the desired properties.

3. The measuring station in the model should be located at least 6 spire heights downstream of the spires. This appears to allow the proper development of the shear layer from the initial disturbances introduced by the spires, and to achieve a sufficient degree of two-dimensionality in the flow.

4. The thickness of the shear layer at 6 spire heights downstream will probably be less than the spire height. The ratio of shear layer thickness to spire height does not seem to be fixed for all spire sizes, and indications are that the ratio decreases for increasing spire height.

4.0 REFERENCES

1. Templin, R. J. — "Interim Progress Note on Simulation of Earth's Surface Winds by Artificially Thickened Wind Tunnel Boundary Layers" NRC, NAE Aero LTR-LA-22. Feb. 1969.

2. Campbell, G. S. Standen, N. M. — "Progress Report II on Simulation of Earth's Surface Winds by Artifically Thickened Wind Tunnel Boundary Layers" NRC, NAE Aero LTR-LA-37. July 1969

3. Yeh, F. F. Nickerson, E. C. — "Air Flow Over Roughness Discontinuity" Project THEMIS, Tech. Rep. No. 8, Fluid Dynamics and Diffusion Laboratory, College of Engineering, Colorado State University, July 1970.

4. Davenport, A. G. Isyumov, N. — "The Application of the Boundary Layer Wind Tunnel to the Prediction of Wind Loading", Paper No. 7, Proceedings of the International Research Seminar on Wind Effects on Buildings and Structures Ottawa, Sept. 1967. University of Toronto Press.

5. Gault, J. D. Gunter, D. E. — "Atmospheric Turbulence Considerations for Future Aircraft Designed to Operate at Low Altitudes". AIAA Paper No. 68-216. Feb. 1968.

6. Berman, S. — "Estimating the Longitudinal Wind Spectrum Near the Ground". Quarterly Journal of the Royal Meteorological Society, Vol. 91, No. 389. July 1965.

7. Standen, N. M. Dalgliesh, W. A. Templin, R. J. — "A Wind Tunnel and Full-Scale Study of Turbulent Wind Pressures on a Tall Building". Presented at the International Conference on Wind Effects on Buildings and Structures, Tokyo, 1971. Available in the National Research Council of Canada DME/NAE Quarterly Bulletin No. 1971(4), January, 1972.

TABLE I

DIMENSIONS OF STANDARD HALF-WIDTH SPIRES

HEIGHT	SPIRE WIDTH
0	0.5000
0.0016	0.3750
0.0111	0.3100
0.0167	0.2933
0.0250	0.2733
0.0417	0.2483
0.0833	0.2100
0.1250	0.1850
0.1667	0.1650
0.2500	0.1350
0.3333	0.1117
0.4167	0.0917
0.5000	0.0750
0.5833	0.0600
0.6667	0.0450
0.7500	0.0333
0.8333	0.0217
0.9167	0.0117
1.0000	0.0

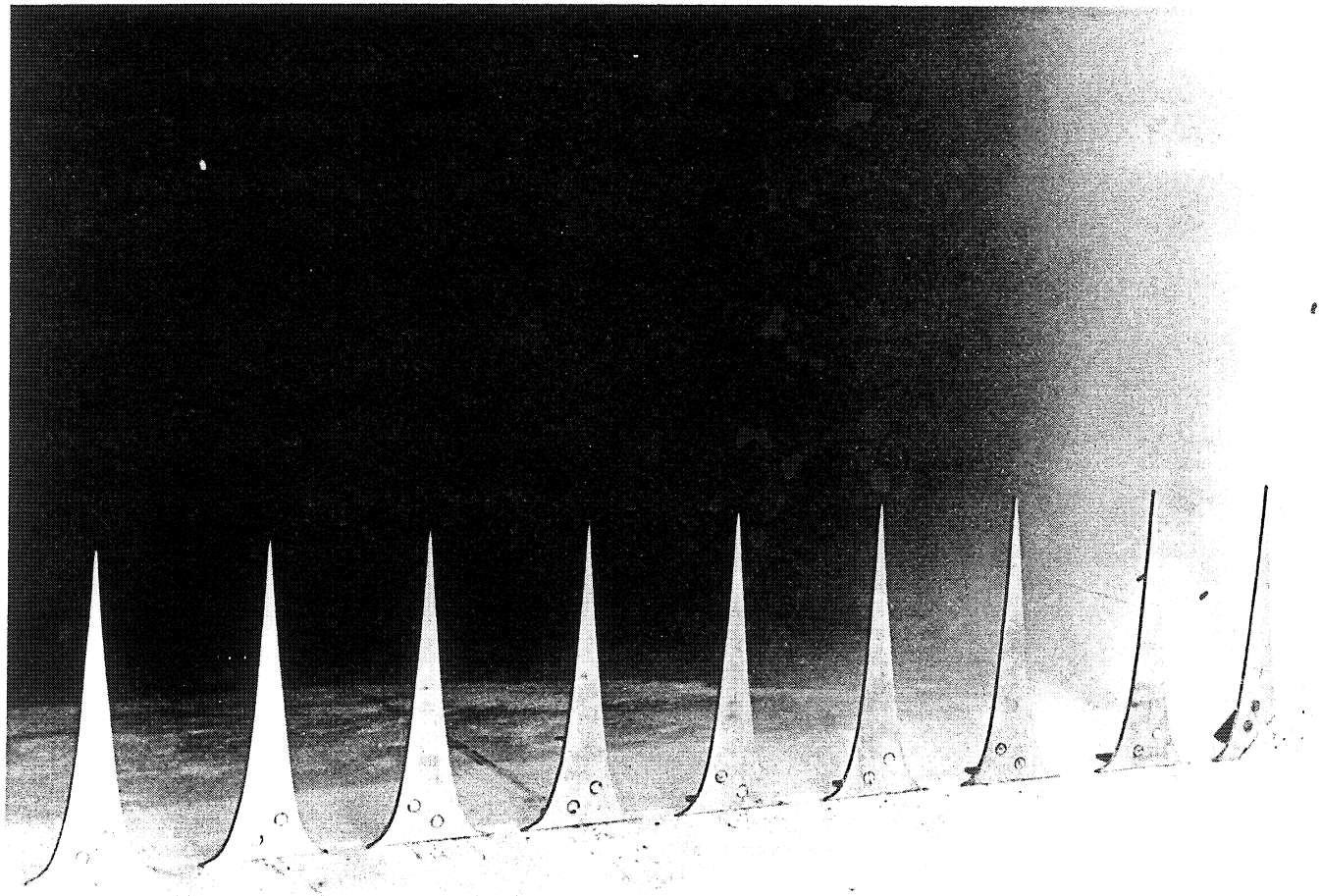

FIG. 1: 6 INCH STANDARD HALF-WIDTH SPIRES

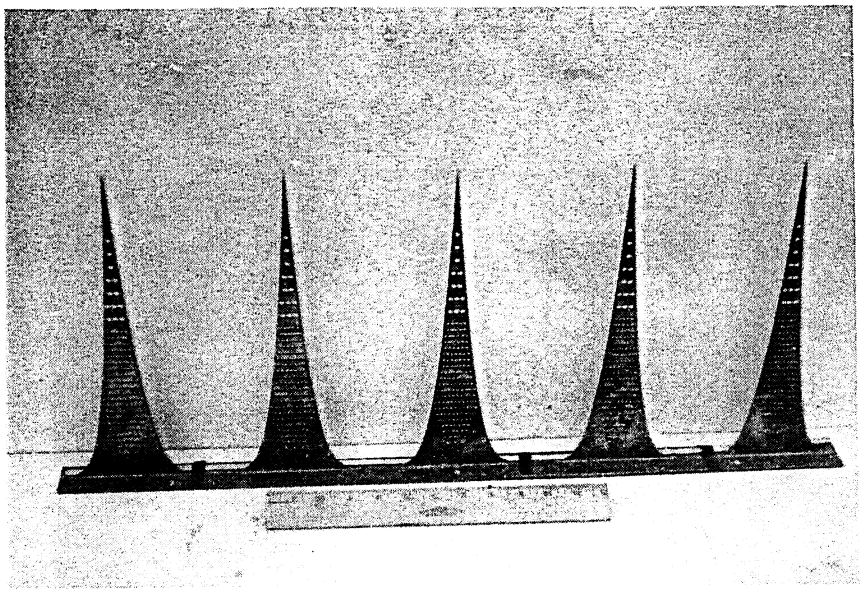

FIG. 2: 12 IN. HALF-WIDTH SPIRES

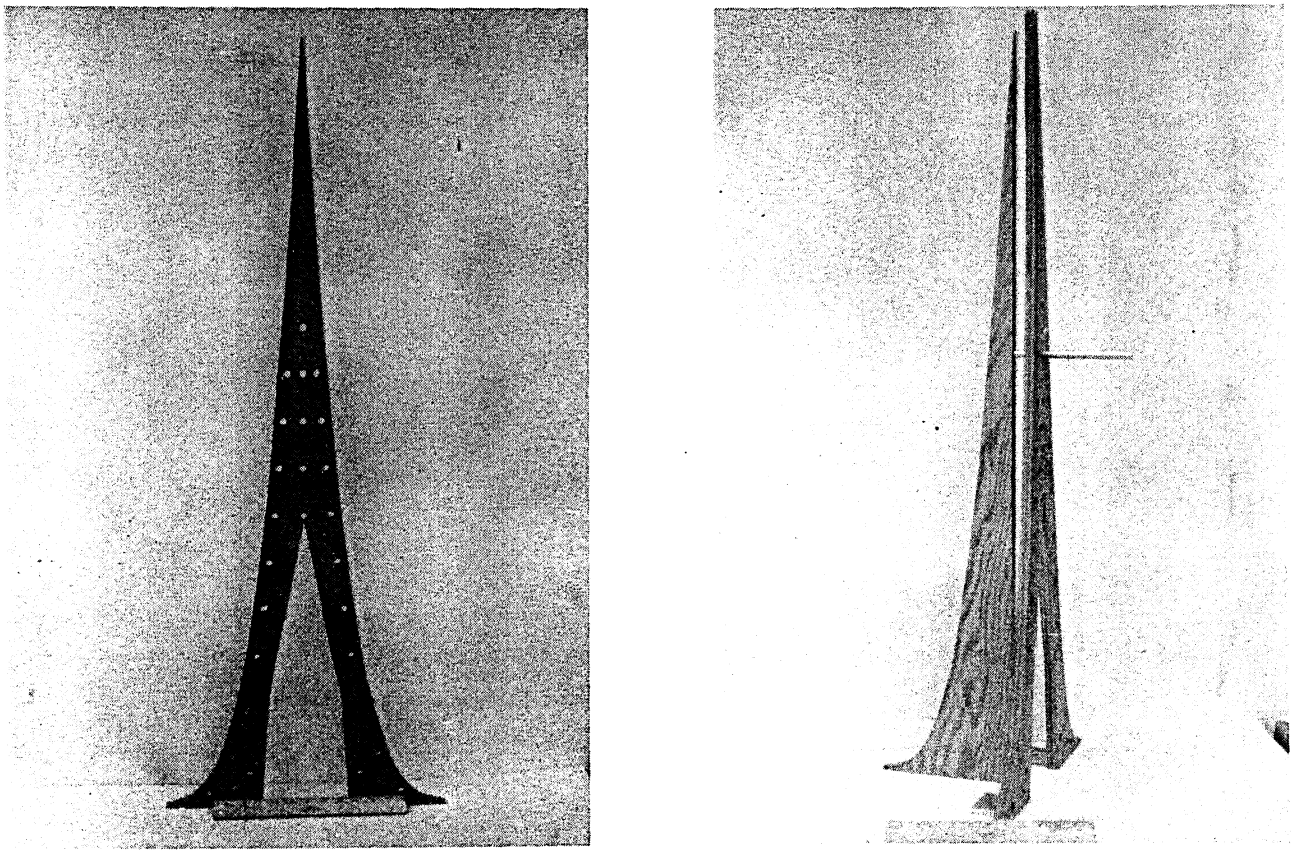

A B

FIG. 3: 4 FT. SPIRES (A) WITH CUTOUT AND (B) WITH SPLITTER

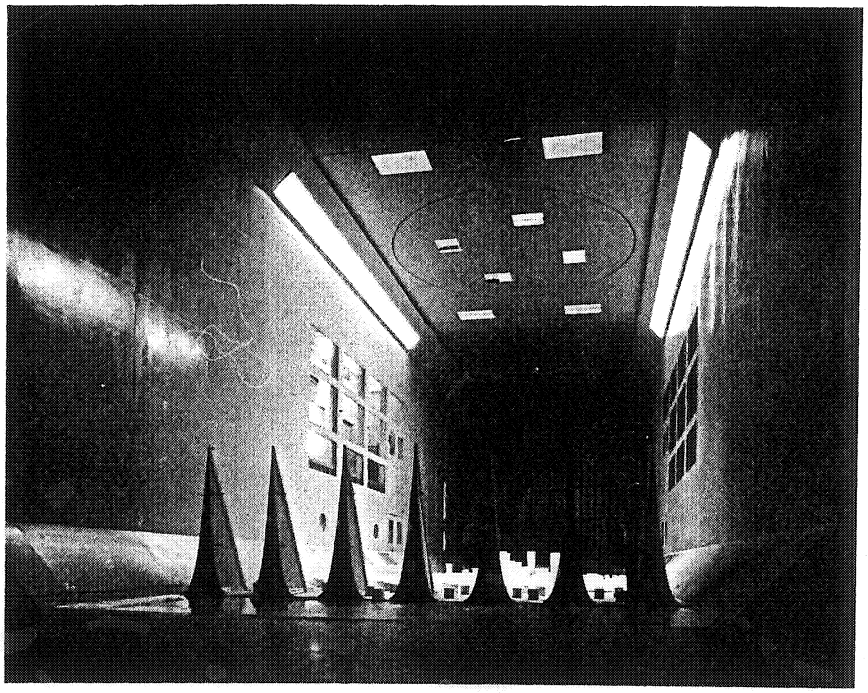

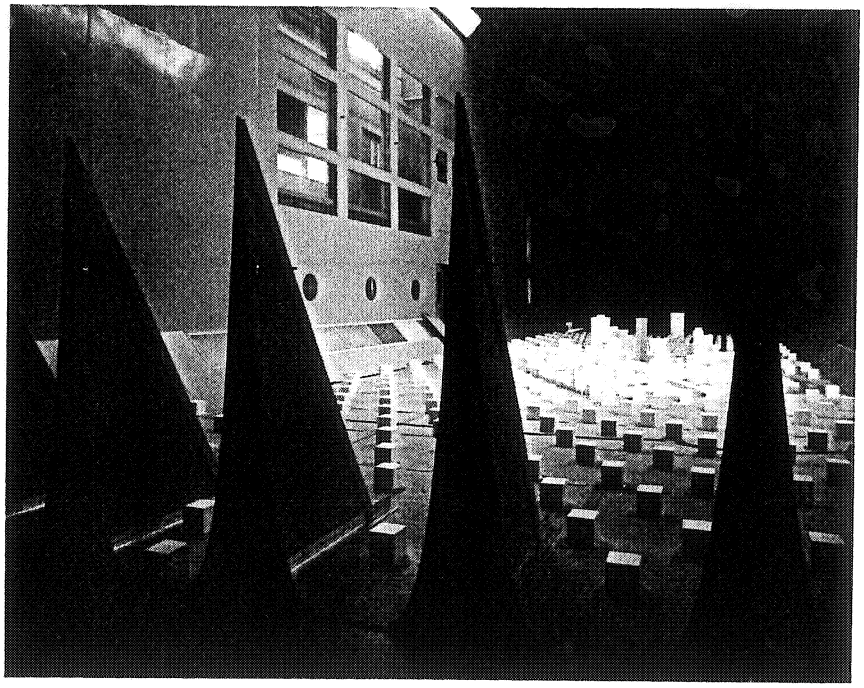

FIG. 4: 7 FT. HALF-WIDTH SPIRES
WITH SPLITTER PLATES
AND BLOCK ROUGHNESS

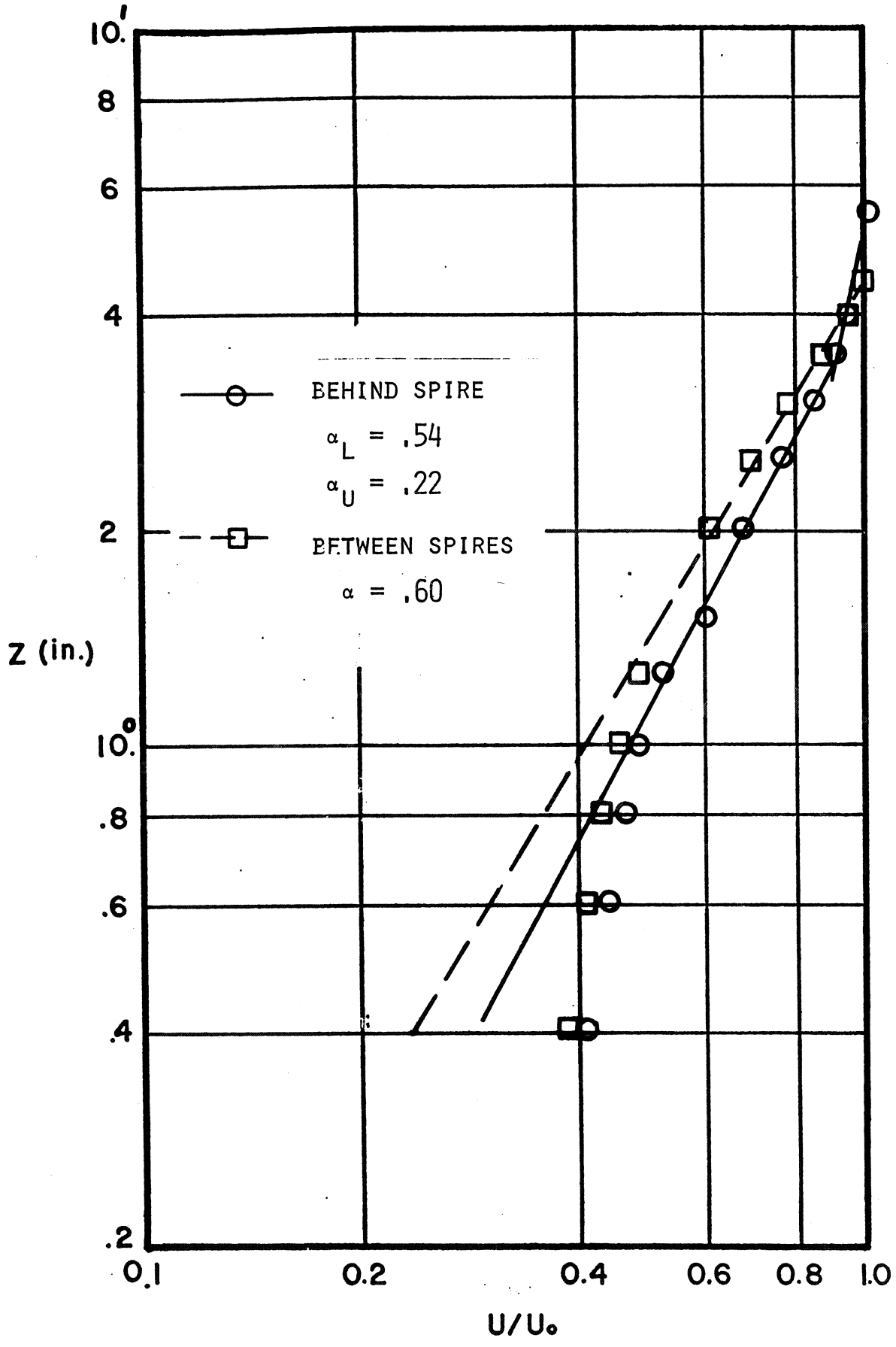

FIG. 5(A) 6 IN. SPIRES, SMOOTH FLOOR;
18 IN. DOWNSTREAM

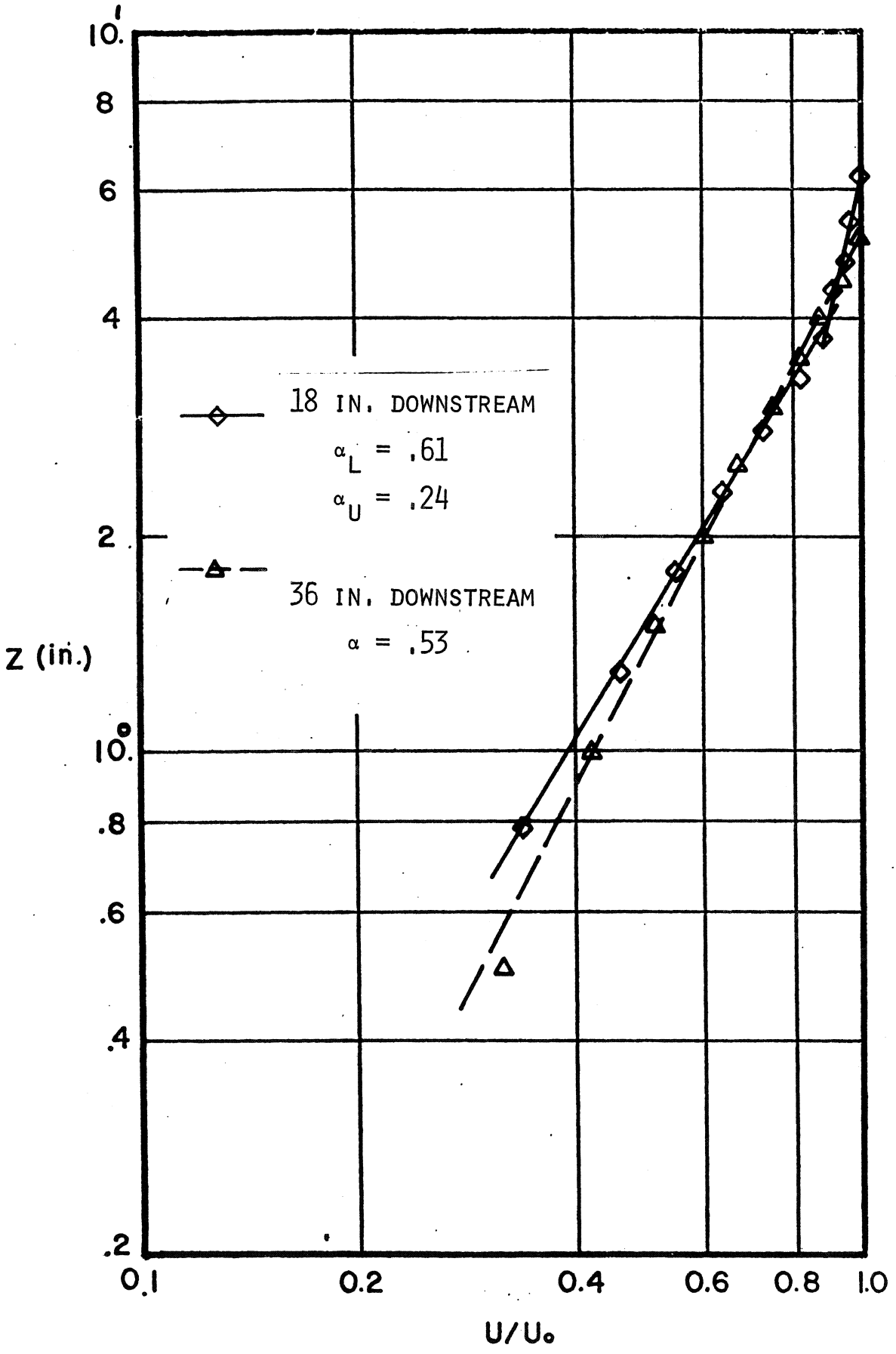

FIG. 5(c) 6 IN. SPIRES, RIVET ROUGHNESS; BEHIND SPIRE

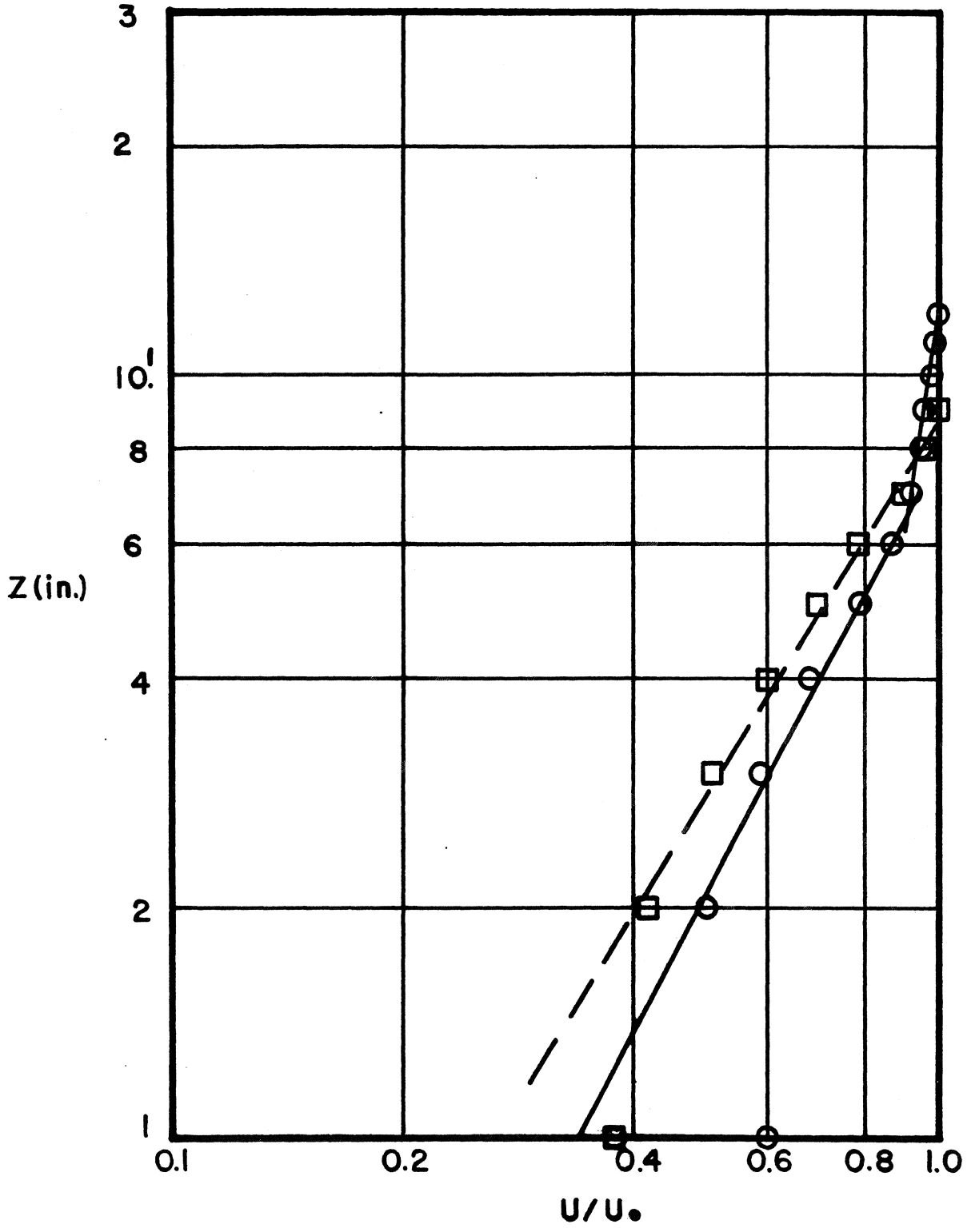

FIG. 6 12 IN. SPIRES, SMOOTH FLOOR; 36 IN. DOWNSTREAM

—⊖— BEHIND SPIRE

α_L = .54

α_U = .22

—⊟— BETWEEN SPIRES

α = .62

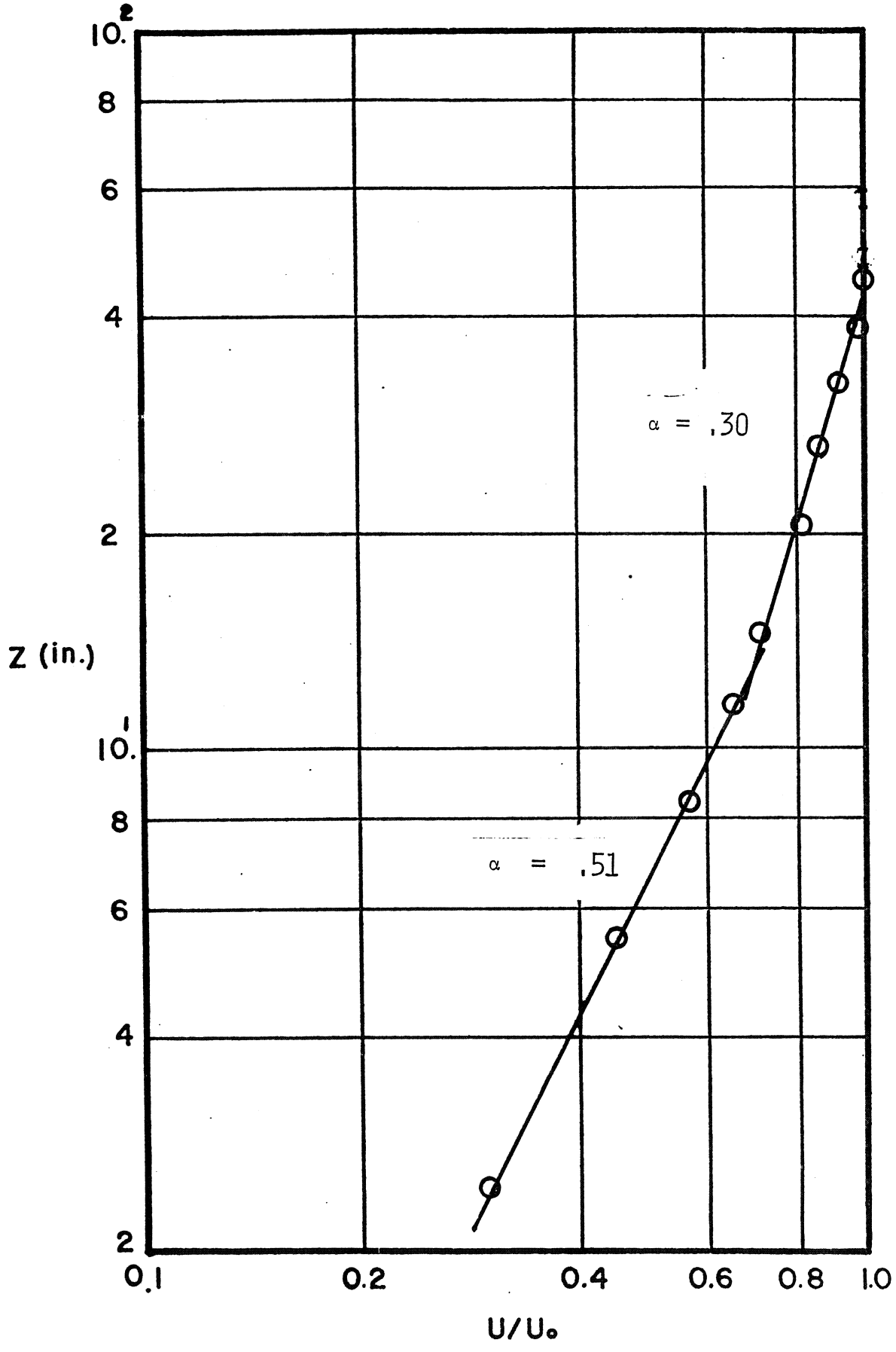

FIG. 7 4 FT. SPIRES, CUBE ROUGHNESS;
24 FT. DOWNSTREAM

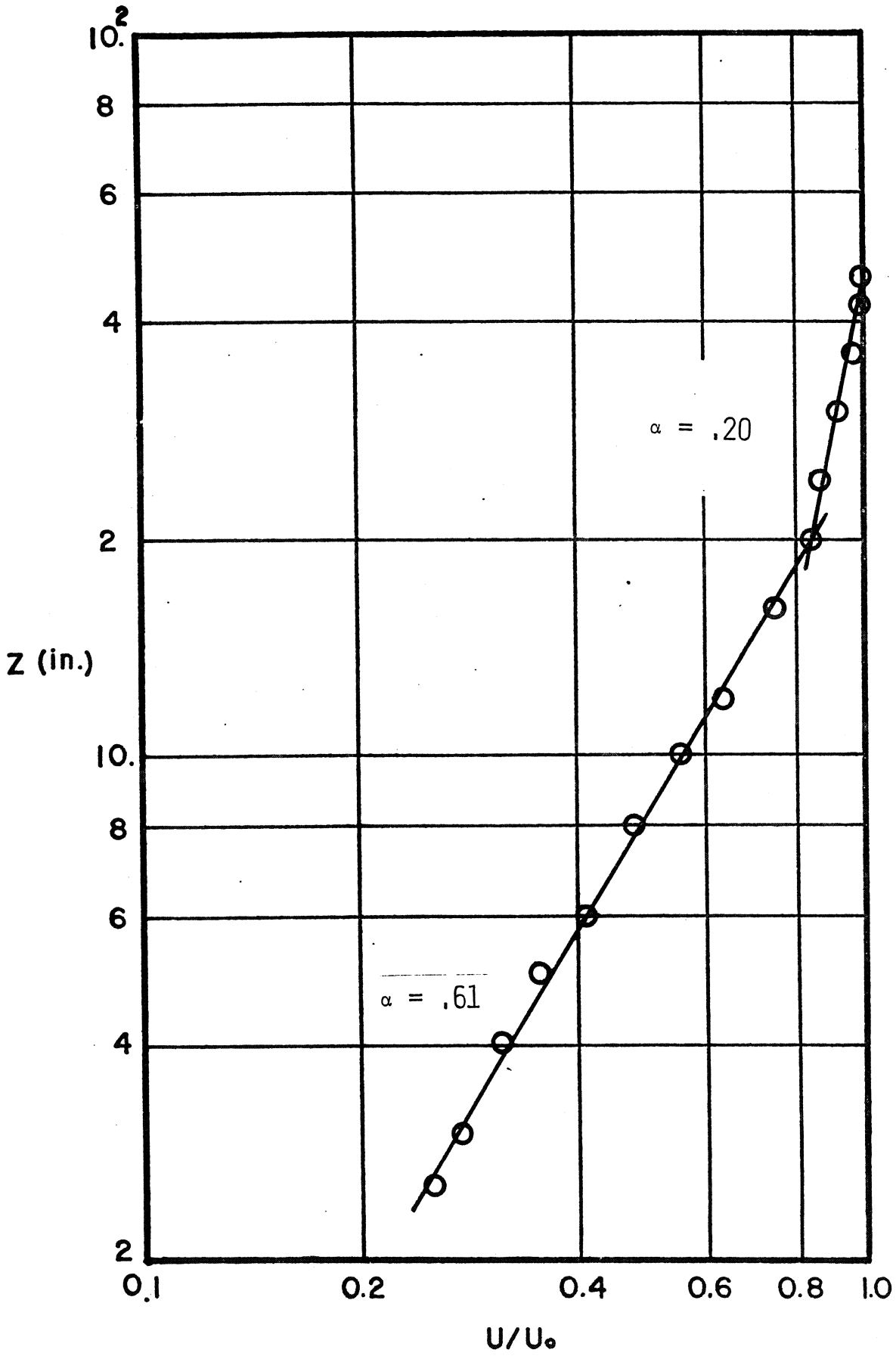

FIG. 8 4 FT. SPIRES, ROUGHNESS AND CITY;
24 FT. DOWNSTREAM

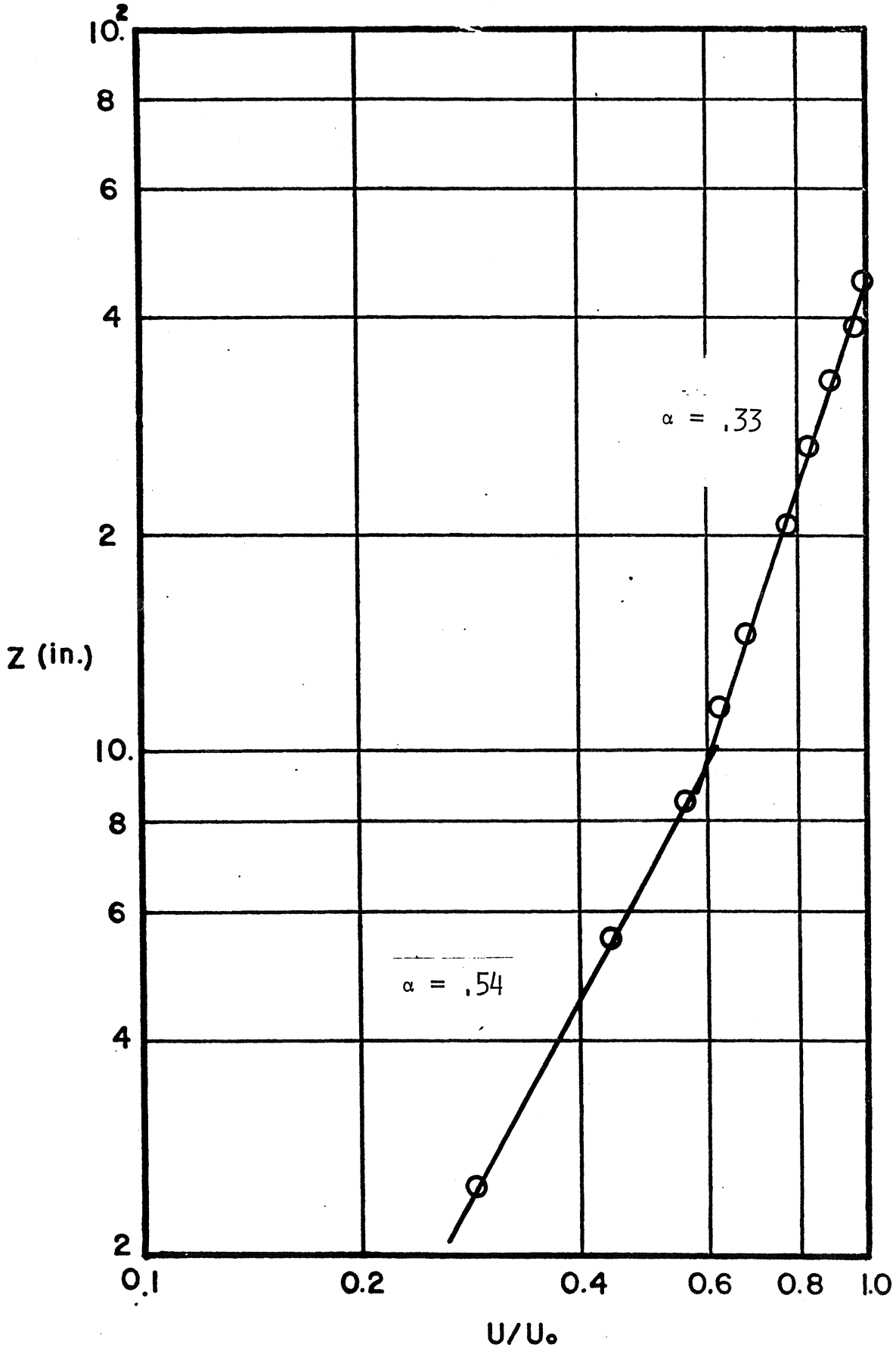

FIG. 9 4 FT. SPIRES WITH SPLITTER PLATE, CUBE ROUGHNESS; 24 FT. DOWNSTREAM

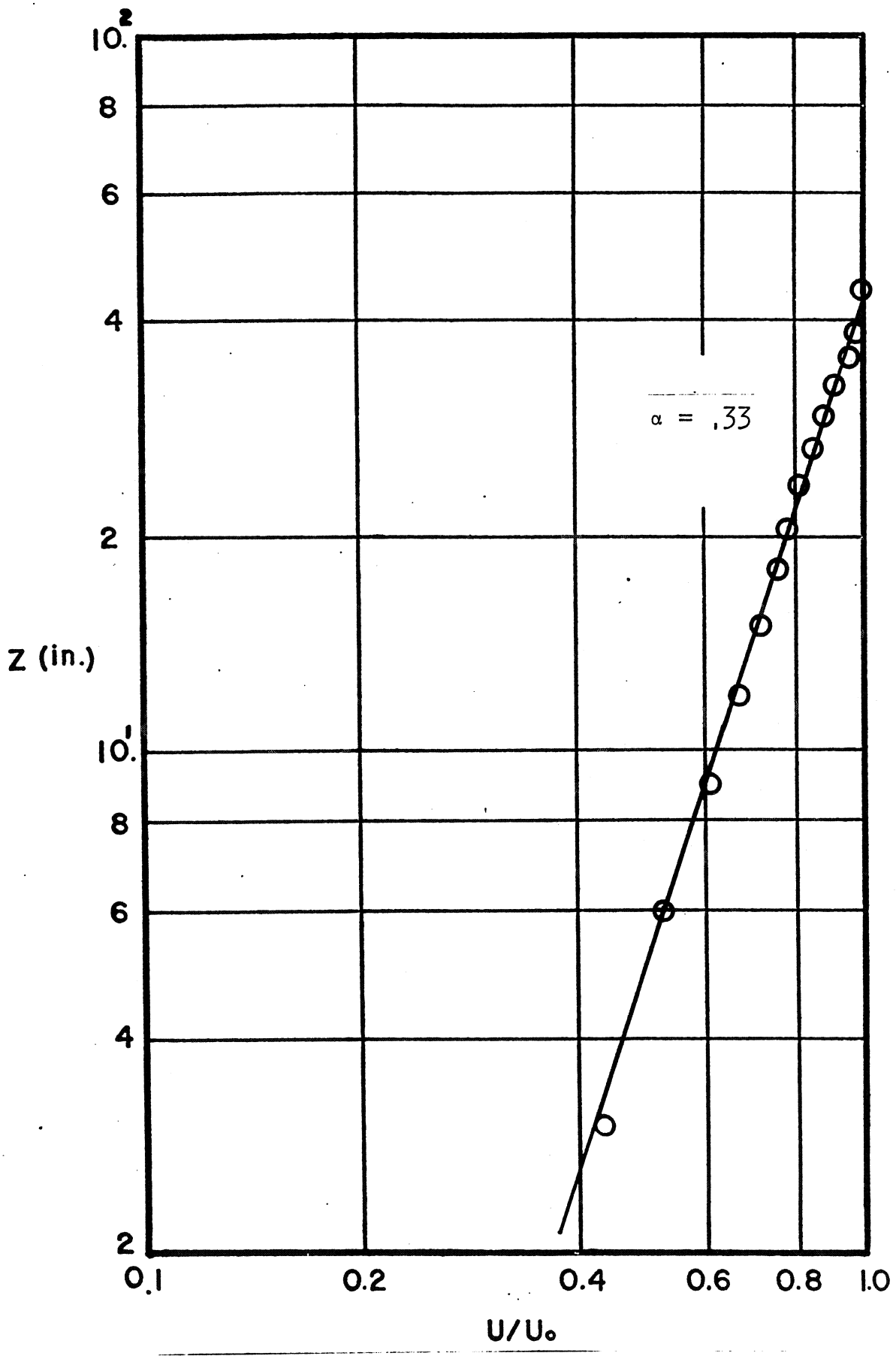

FIG. 10 4 FT. SPIRES WITH SPLITTER PLATE
9 ROWS OF CUBE ROUGHNESS REMOVED;
24 FT. DOWNSTREAM

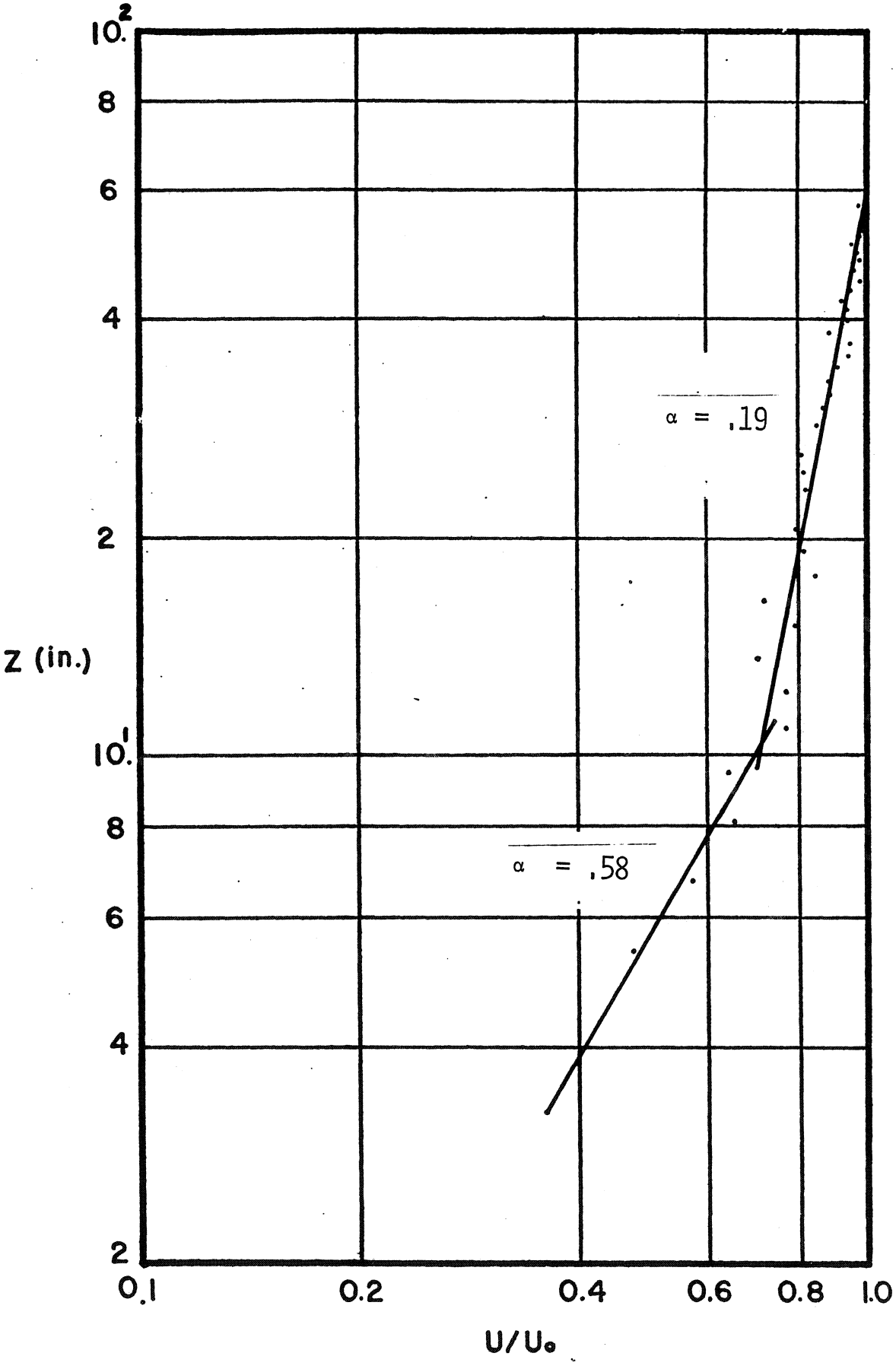

FIG. 11 7 FT. SPIRES WITH SPLITTER PLATE, CUBE ROUGHNESS; 40 FT. DOWNSTREAM

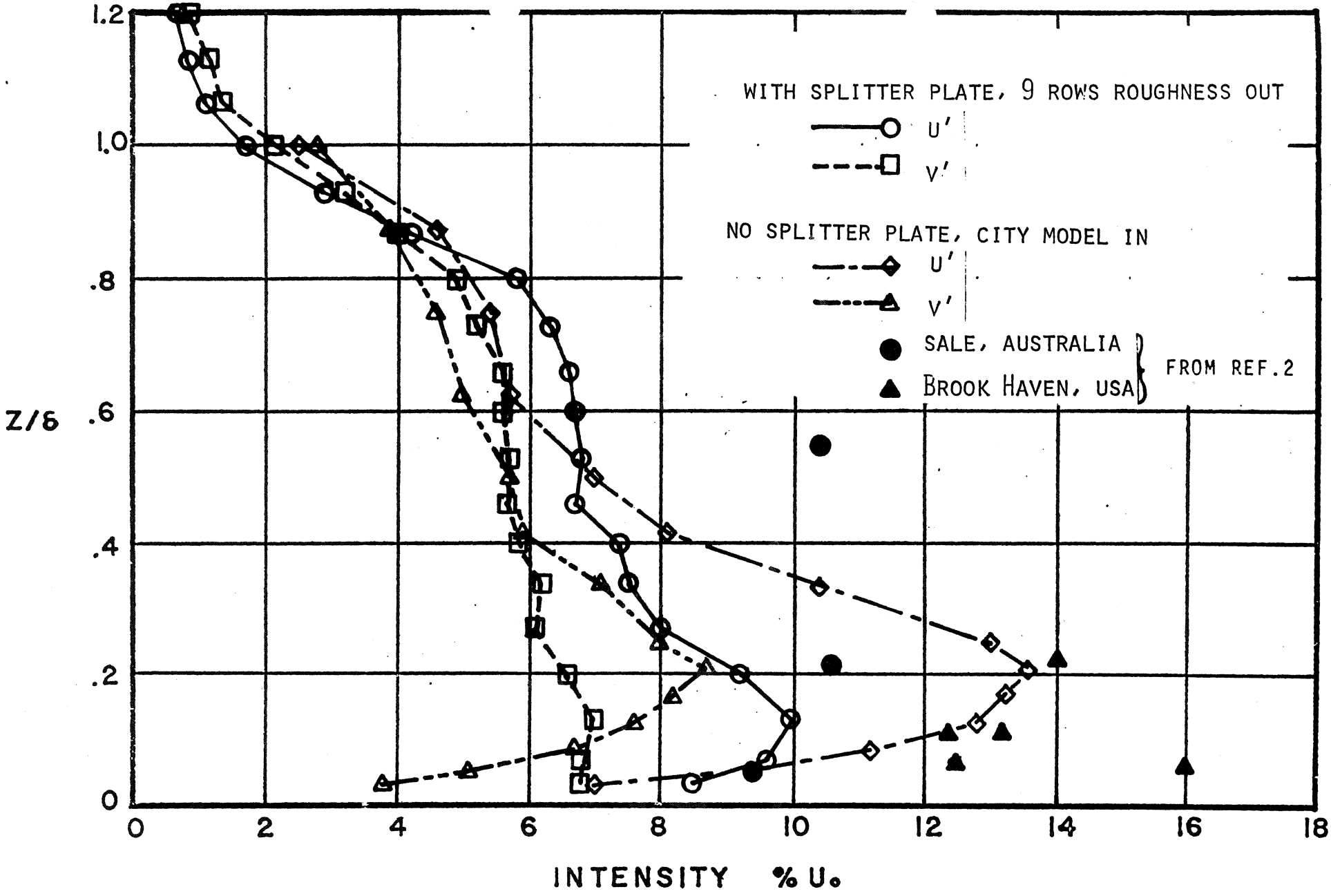

FIG. 13(B) TURBULENCE INTENSITIES BEHIND 4 FT. SPIRES

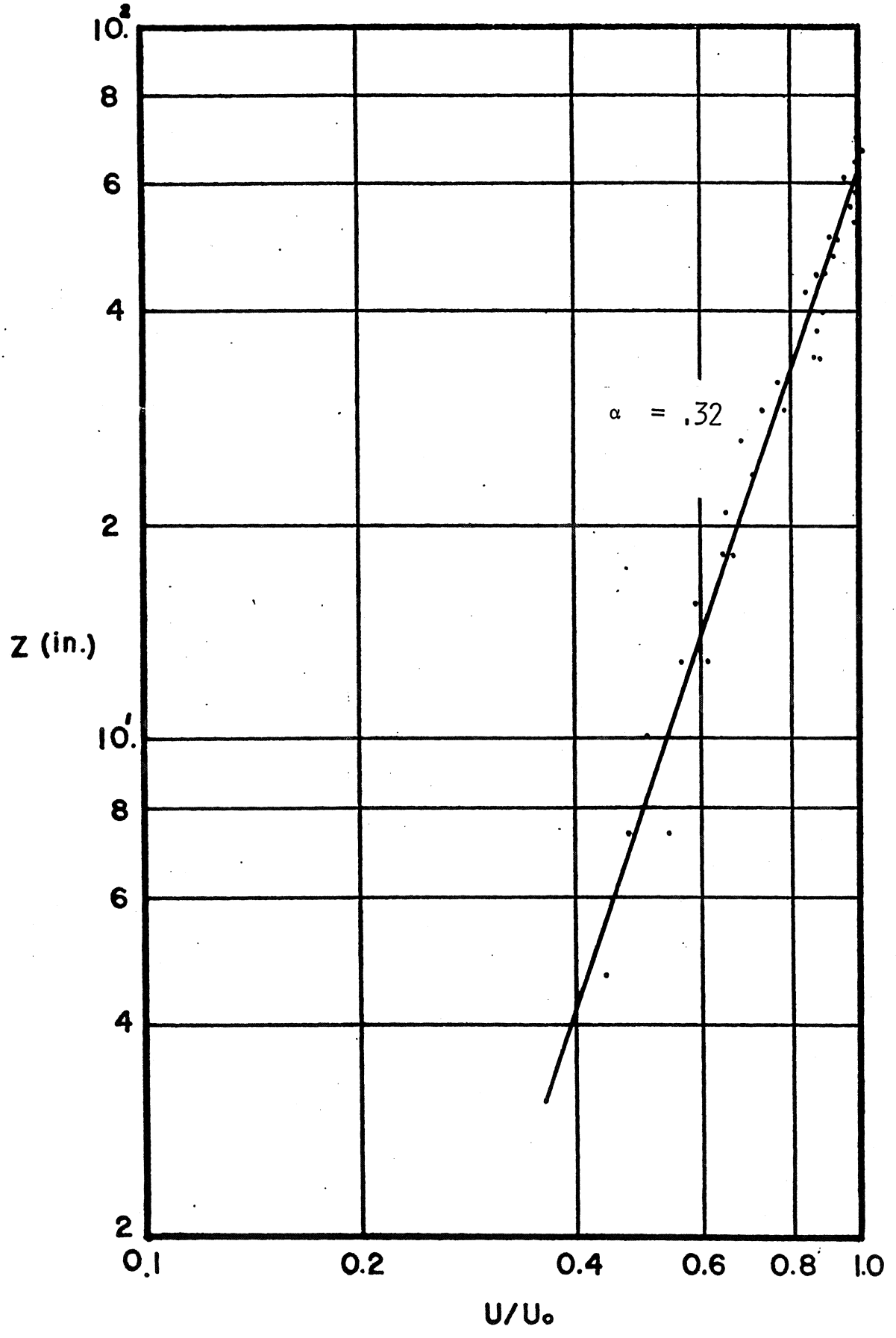

FIG. 12 7 FT. SPIRES WITH SPLITTER PLATE, ROUGHNESS AND CITY MODEL; 40 FT. DOWNSTREAM

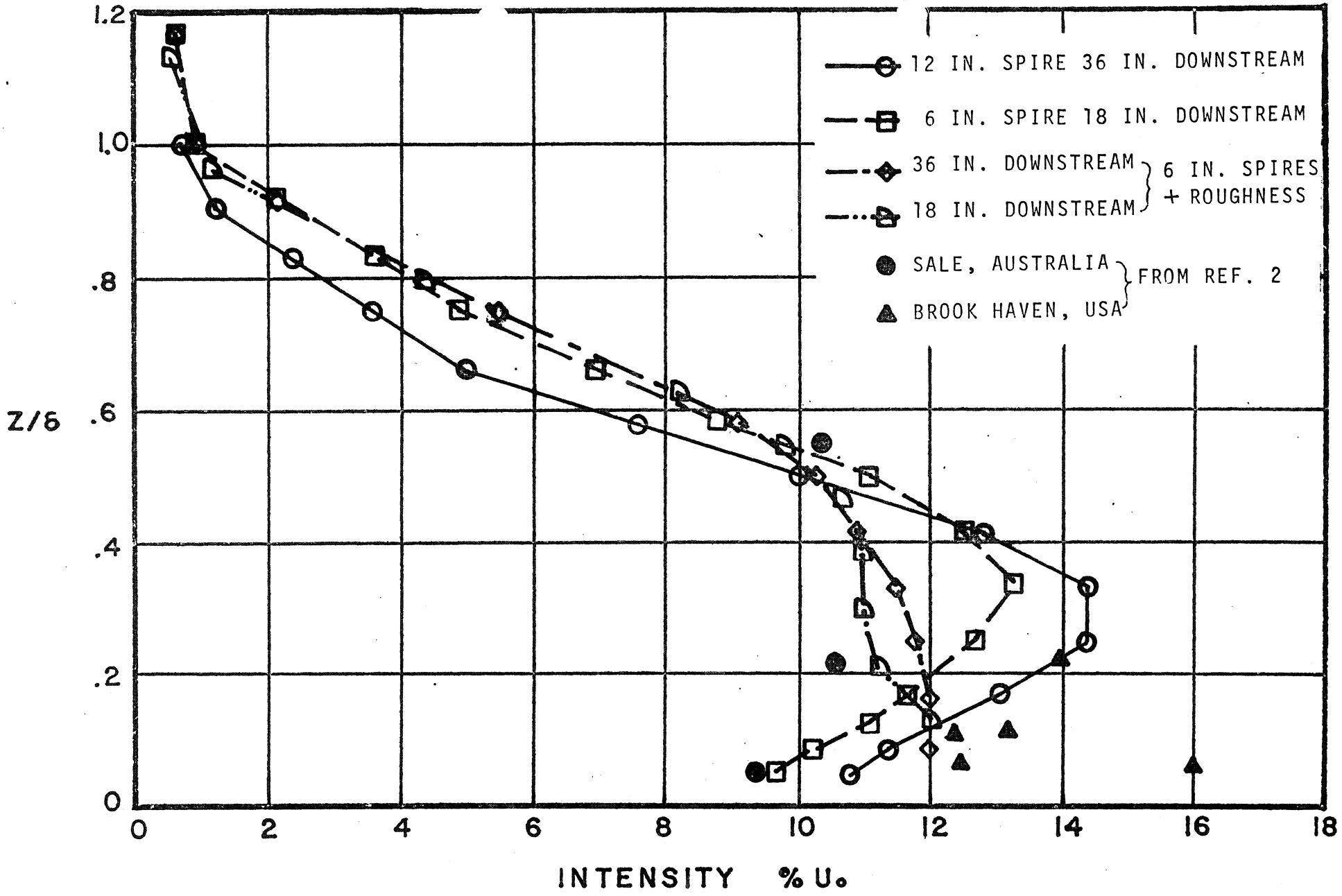

FIG. 13(A) INTENSITY OF LONGITUDINAL TURBULENCE COMPONENT

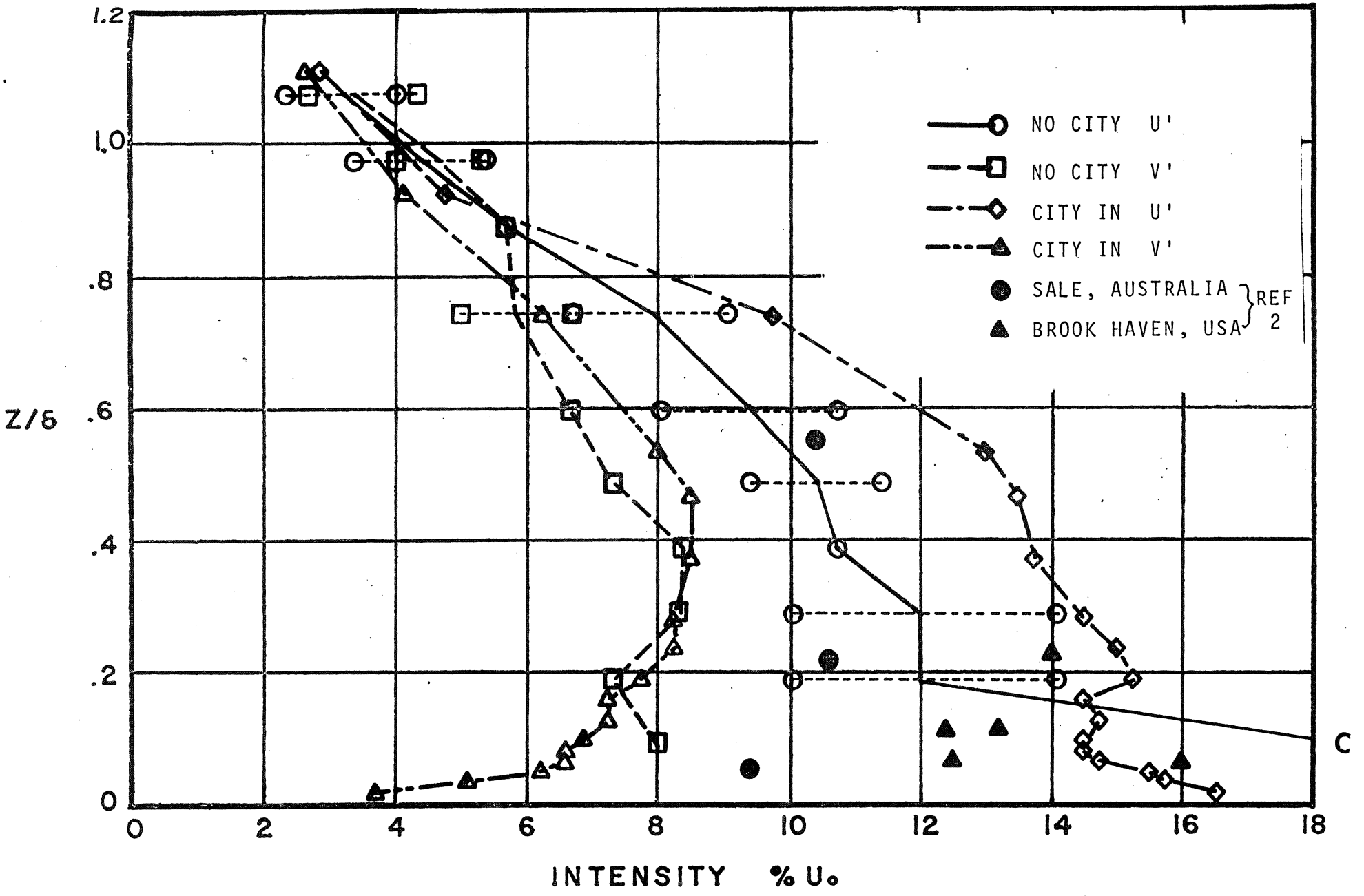

FIG. 13(c) TURBULENCE INTENSITIES BEHIND 7 FT. SPIRES

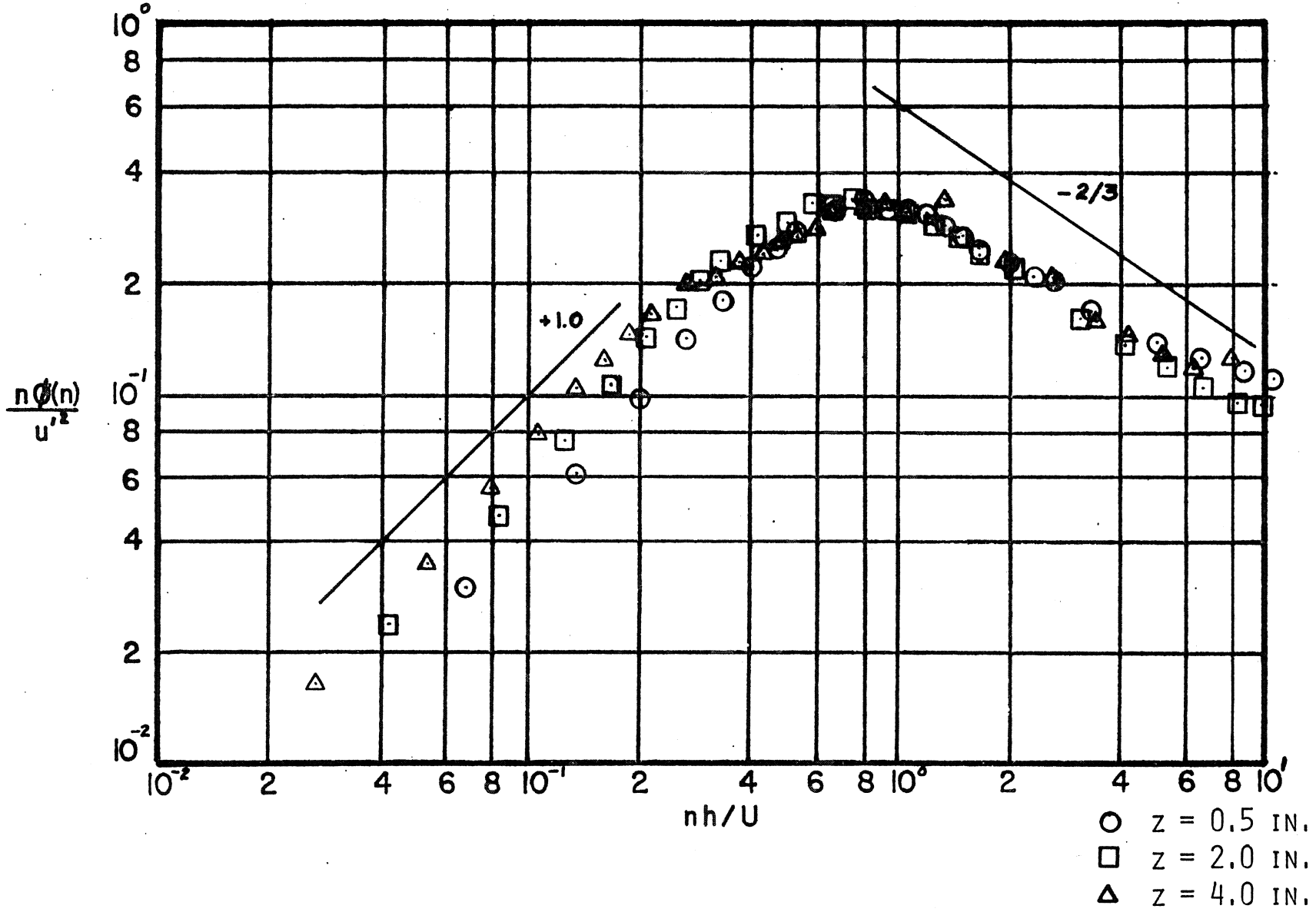

FIG. 14(A) POWER SPECTRAL DENSITIES - U' TURBULENCE
6 IN. SPIRES, NO ROUGHNESS
18 IN. DOWNSTREAM

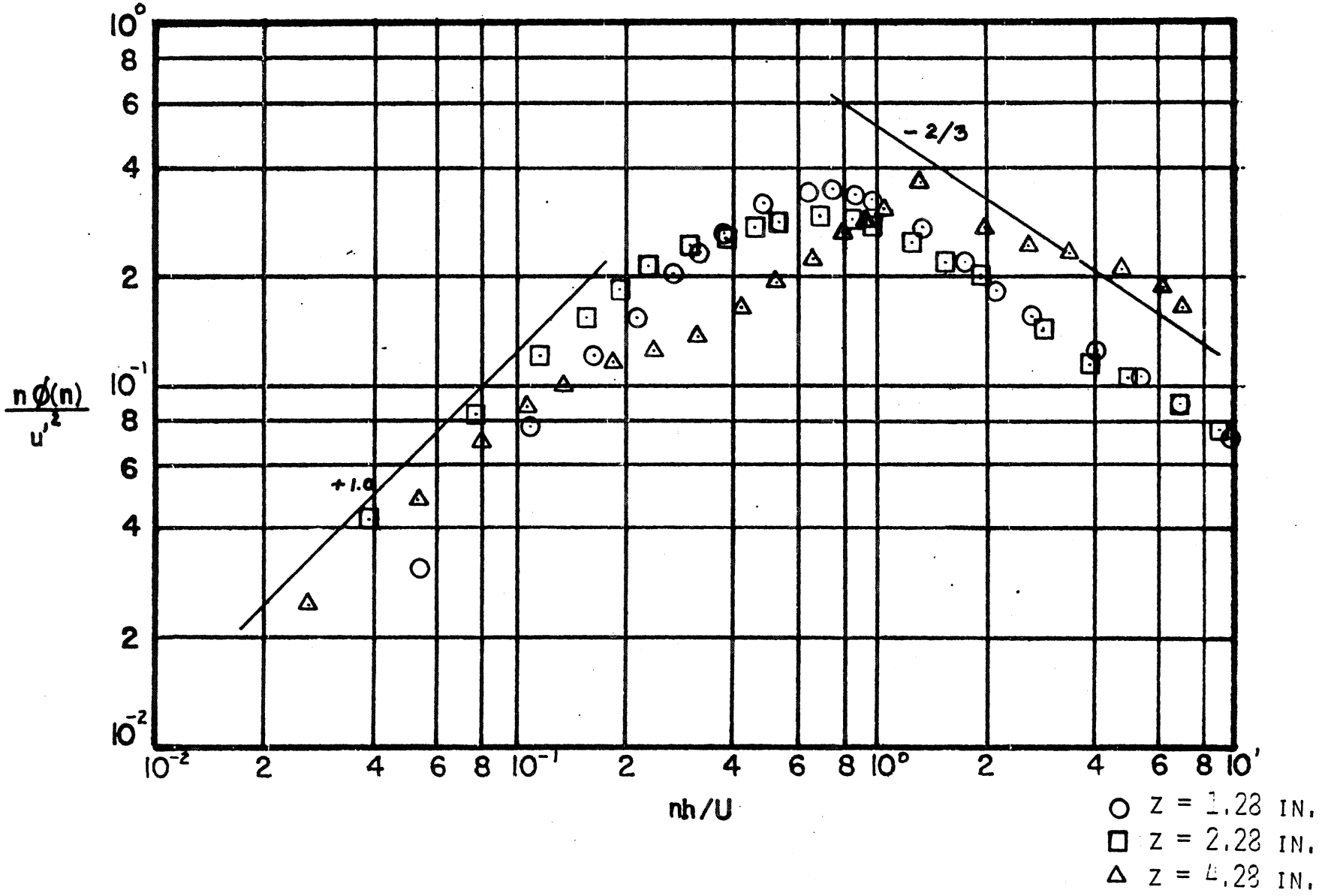

FIG. 14(B) POWER SPECTRAL DENSITIES - U' TURBULENCE
6 IN. SPIRES AND ROUGHNESS
18 IN. DOWNSTREAM

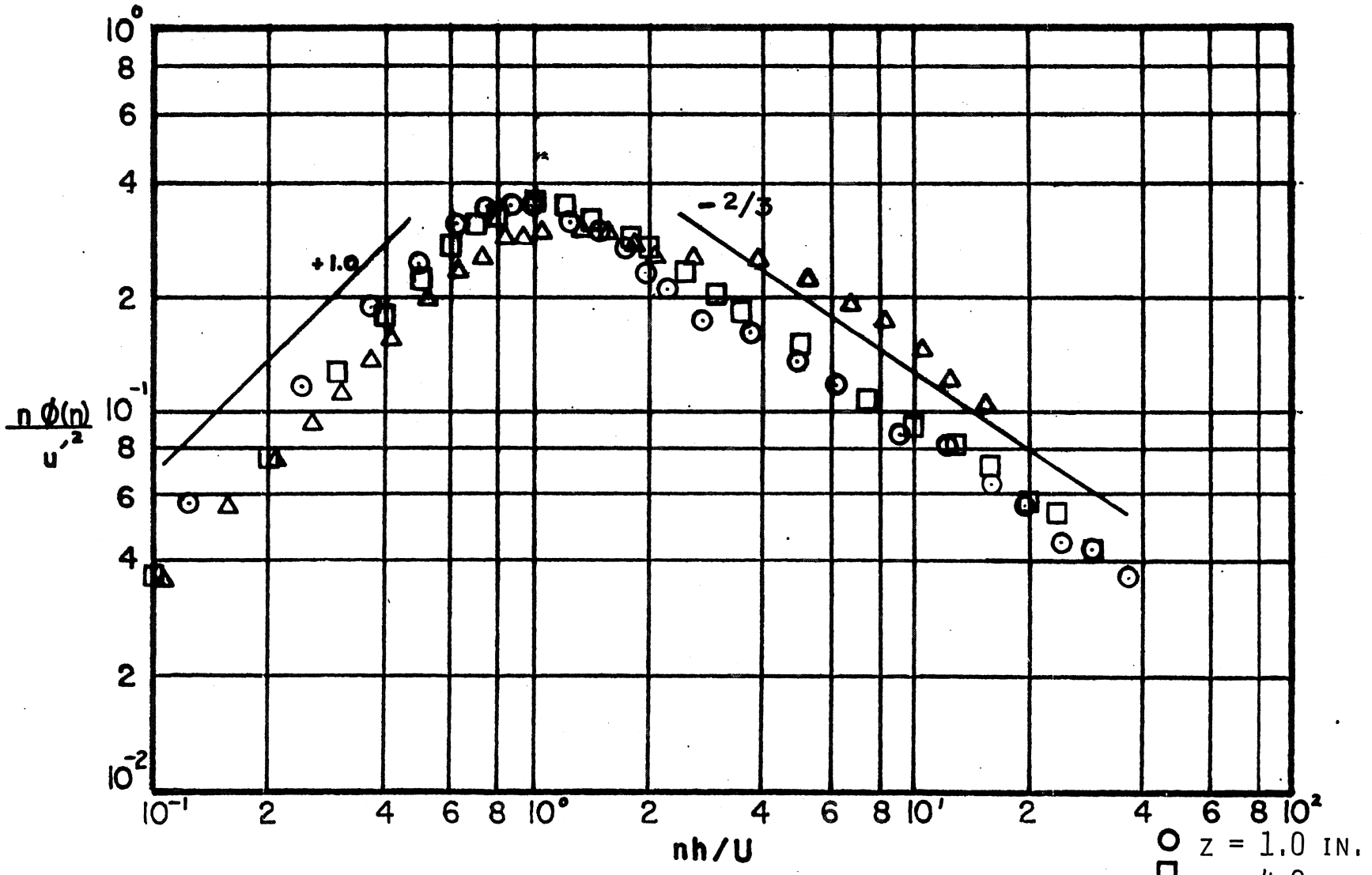

FIG. 14(c) POWER SPECTRAL DENSITIES - U' TURBULENCE
12 IN. SPIRES, BEHIND SPIRE
36 IN. DOWNSTREAM

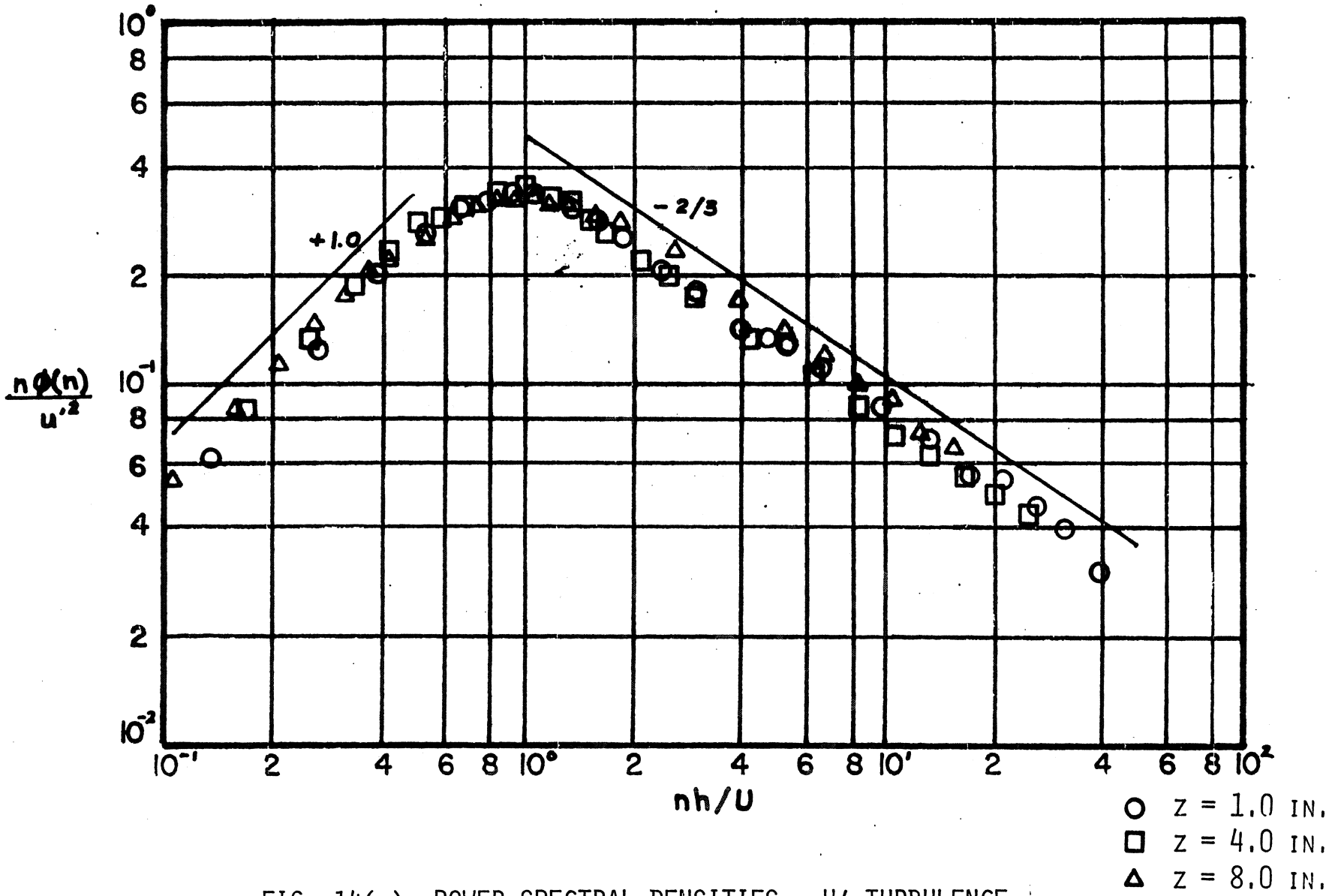

FIG. 14(D) POWER SPECTRAL DENSITIES - U' TURBULENCE
12 IN. SPIRES, BETWEEN SPIRES,
36 IN. DOWNSTREAM

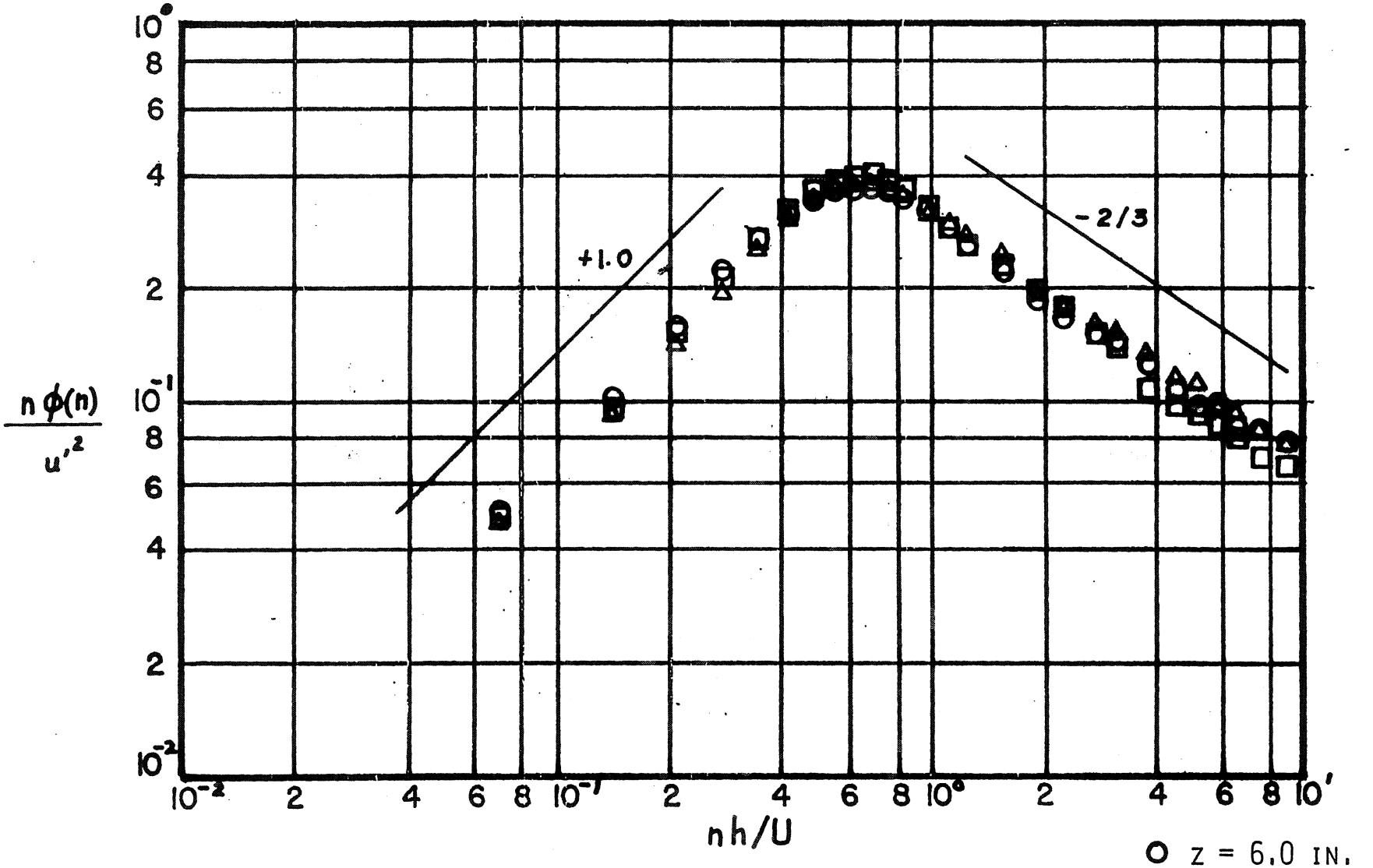

FIG. 14(E) POWER SPECTRAL DENSITIES - U' TURBULENCE
4 FT. SPIRES, NO CITY

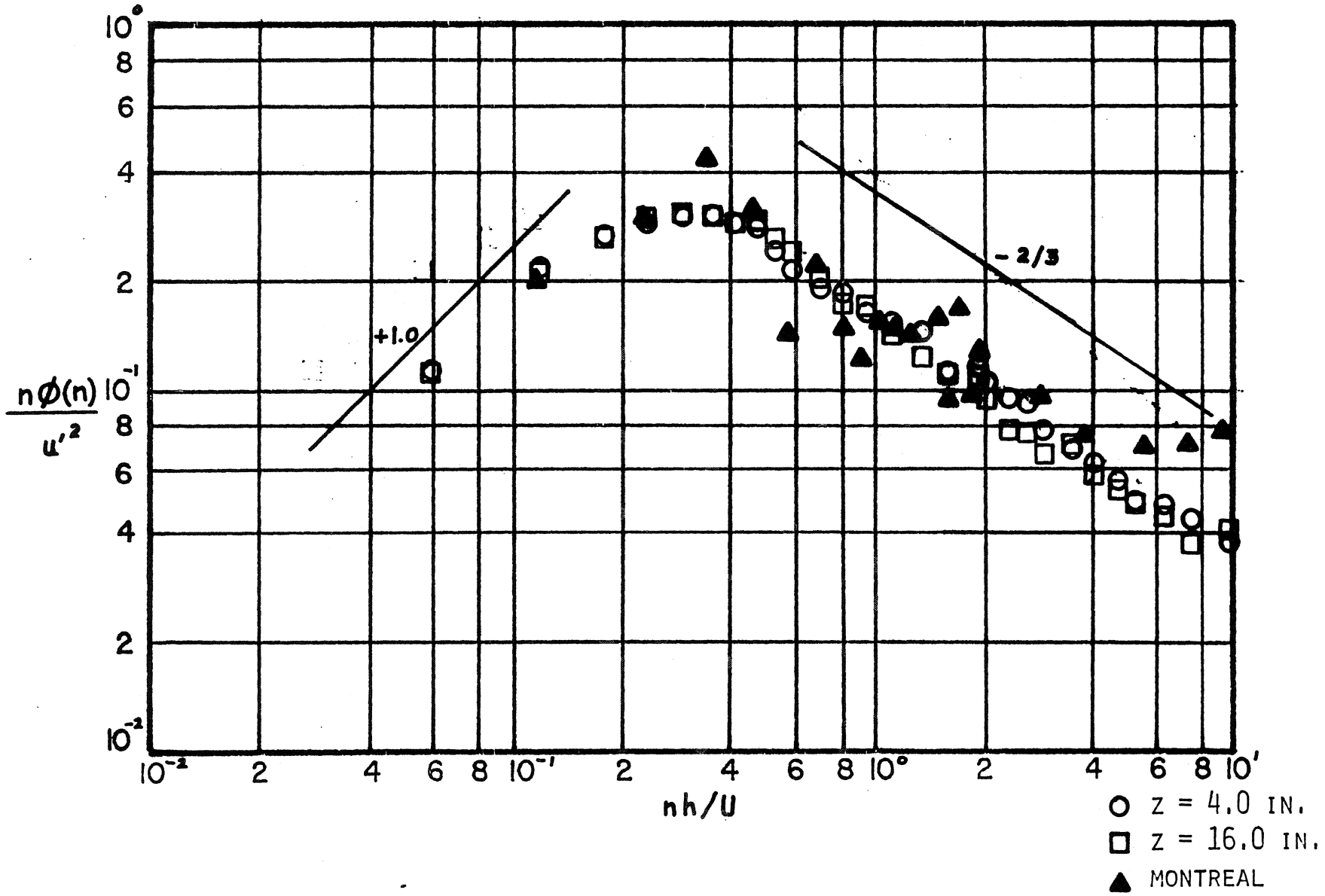

FIG. 14(F) POWER SPECTRAL DENSITIES - U' TURBULENCE
4 FT. SPIRES, CITY IN

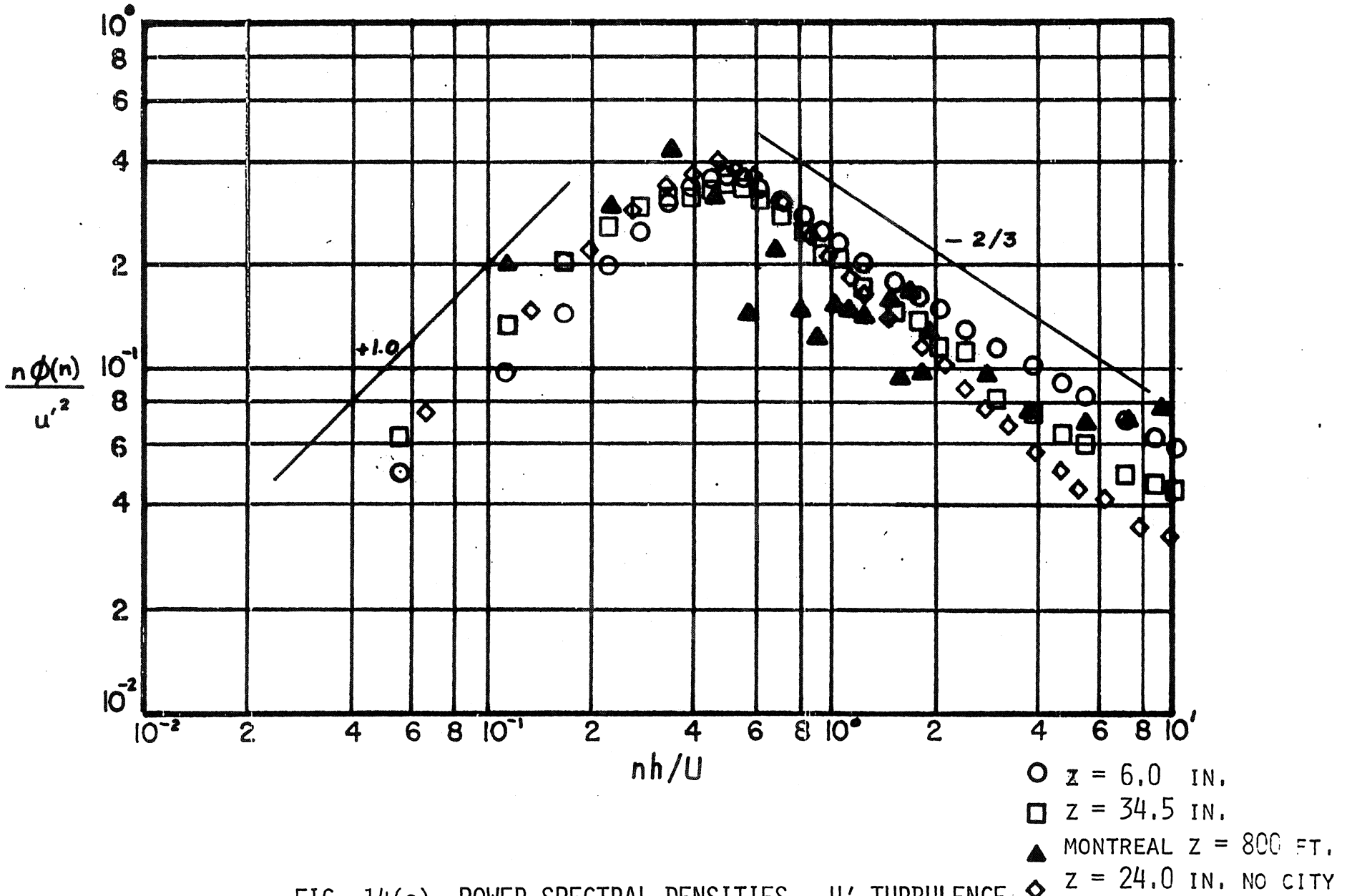

FIG. 14(G) POWER SPECTRAL DENSITIES - U' TURBULENCE
7 FT. SPIRES

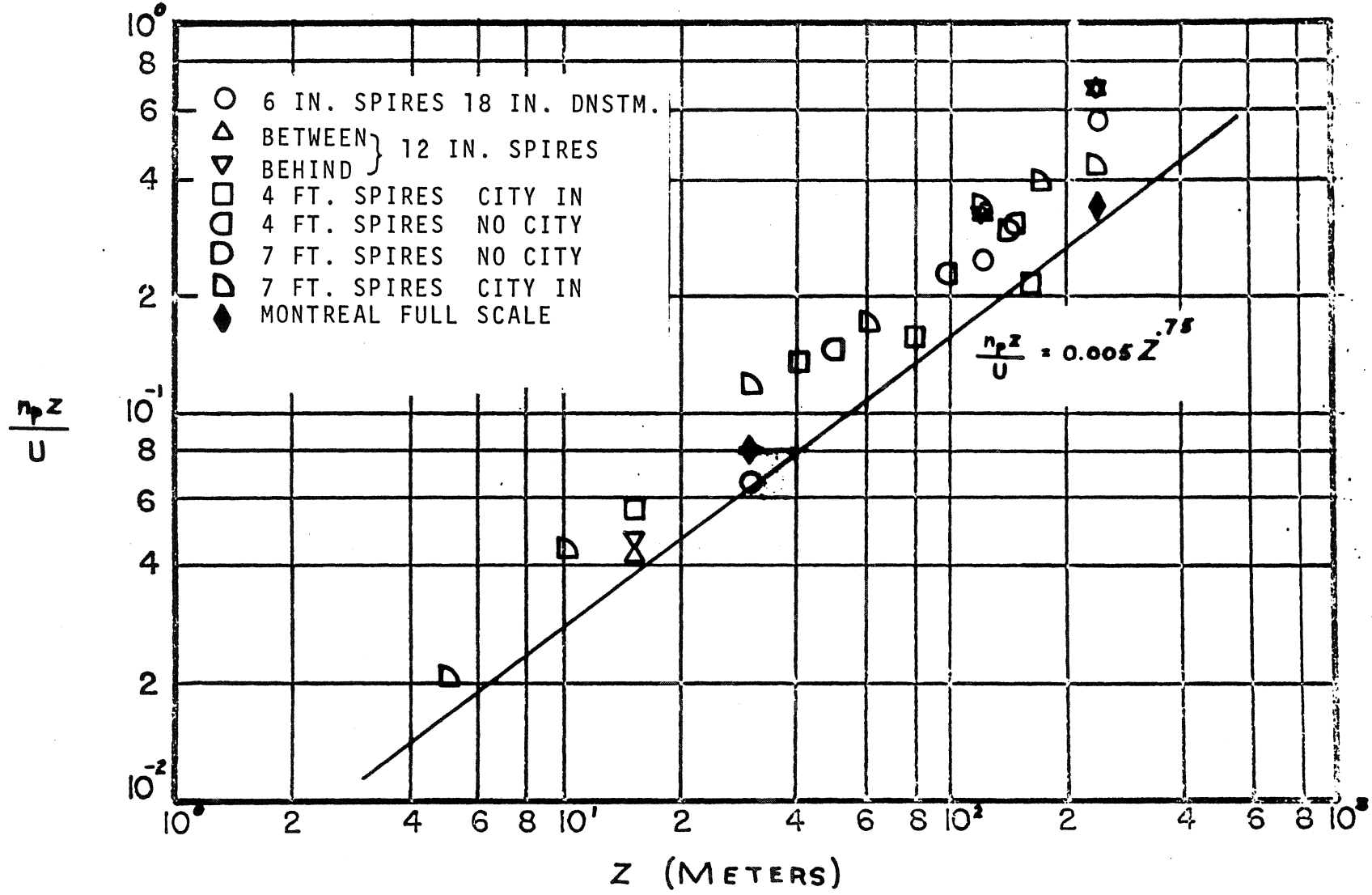

FIG. 15 VARIATION OF SPECTRAL PEAK FREQUENCY WITH HEIGHT